International Journal of Biological Macromolecules 320 (2025) 145870

Contents lists available at ScienceDirect

International Journal of Biological Macromolecules

journal homepage: www.elsevier.com/locate/ijbiomac

Designing of biosafe, multifunctional alginate-nanoclay hydrogels for environmental applications: structure, swelling properties, and cadmium sorption

Nataliia Guzenko [a,b], Olena Goncharuk [a,c], Yurii Samchenko [c], Konrad Terpiłowski [d], Katarzyna Grygorczuk-Płaneta [a], Svitlana Dybkova [c], Bartosz Kondracki [e], Katarzyna Szewczuk-Karpisz [a,*]

[a] Institute of Agrophysics, Polish Academy of Sciences, Doświadczalna 4, 20-290 Lublin, Poland
[b] Chuiko Institute of Surface Chemistry, NAS of Ukraine, 17 General Naumov str., 03164 Kyiv, Ukraine
[c] F.D. Ovcharenko Institute of Biocolloidal Chemistry, NAS of Ukraine, 42 Vernadskogo Blvd., 03142 Kyiv, Ukraine
[d] Maria Curie-Sklodowska University, M.C. Sklodowska Sq.3, 20-031 Lublin, Poland
[e] Chair and Department of Cardiology, Medical University in Lublin, Jaczewskiego 8 (SPSK Nr 4), 20-954 Lublin, Poland

ARTICLE INFO

Keywords:
Alginate-based hydrogels
Layered nanoclays
Montmorillonite
Laponite
Swelling
Heavy metals sorption

ABSTRACT

Composite hydrogels (HGs) based on sodium alginate (Alg), with nanoclay montmorillonite (MMT) and LaponiteRD (Lap) fillers, were synthesized using ionic cross-linking with calcium ions (Ca^{2+}). The HGs structure was investigated by SEM-EDX, XRD, and FTIR, whereas cation exchange capacity (CEC) and variable surface charge were determined using potentiometric titration. The influence of filler content, cross-linking agent concentration, and pH on the swelling and sorption capacity towards cadmium ions (Cd^{2+}) of HGs was analyzed in detail. The cross-linking agent concentration influenced the swelling mechanism of the alginate-based composites with clays as well as their specific type of water diffusion based on the Fick equation. The $CaCl_2$ concentration (C_{CaCl2}) of 0.3–0.5 wt% was found as optimal for synthesizing mechanically stable HGs with a large swelling degree and sorption ability for Cd^{2+} ions. The sorption capacities calculated based on the Langmuir model were 1.36, 1.19, and 1.33 mmol/g for Alg, Alg/20%MMT, and Alg/20%Lap synthesized using 0.3 wt% $CaCl_2$, respectively. The in vitro tests on genotoxicity and cytotoxicity of HGs, performed using the mouse fibroblast cell culture L-929, proved the biosafety of the developed composites for the environment.

1. Introduction

Contamination with heavy metals, primarily caused by wastewater emissions from industrial enterprises, has become an extremely serious environmental problem. These biologically non-essential species are extremely toxic to aquatic organisms and humans when they penetrate food chains [1–5]. Lead (Pb) and cadmium (Cd) are among the most widespread and intractable environmental threats to public health [2,3]. Cd, originating from industrial processes, agricultural practices, and mining, can persist in ecosystems for extended periods and pose severe risks to human health, biodiversity, and agricultural productivity [3–7]. The International Agency for Research on Cancer (IARC) classifies Cd as a Group 1 carcinogen, associating it with lung and prostate cancers. Ingested Cd, primarily through contaminated food and water, accumulates in various organs, where it can cause irreversible damage [2]. According to the World Health Organization (WHO) guidelines, the maximum allowable concentration of Cd in drinking water is 0.003 mg/L, while strict limits are also applied to the Cd levels in wastewater discharges due to its high toxicity and environmental persistence [3]. Exceeding this permissible concentration can cause health problems such as kidney dysfunction [4], bone damage (Itai-Itai disease) [5], and carcinogenicity [6]. In plants, Cd interferes with photosynthesis, reduces chlorophyll production, and negatively affects root elongation [7].

Recent studies on soils found dangerous Cd levels in various regions worldwide [8–22]. In China, a large-scale study across 3388 agricultural sites revealed widespread Cd pollution. In Hunan Province, China, Cd exceeded the safety thresholds in 16.1 % of agricultural land samples. In the upper Yangtze River region, Wushan County, China, the ecological

* Corresponding author.
E-mail address: k.szewczuk-karpisz@ipan.lublin.pl (K. Szewczuk-Karpisz).

https://doi.org/10.1016/j.ijbiomac.2025.145870
Received 2 March 2025; Received in revised form 30 June 2025; Accepted 7 July 2025
Available online 8 July 2025

risk assessment showed a potential ecological risk (PER) value of 2051, far exceeding the high risk threshold of 1200 [8–12]. A soil study in Hamedan, Iran, assessed the distribution of Cd in different soils cultivated for wheat, which was in the range of 1.30–2.22 mg/kg. Cd accumulation in wheat plants reached 1.08 mg/kg in roots, 0.65 mg/kg in stems, and 0.91 mg/kg in grains [13]. In Tangail District, Bangladesh, the average concentration of Cd in topsoil was 2.17 mg/kg. All 60 examined samples were classified as highly contaminated [14]. In Japan, Cd was considered one of the most harmful metals, and its content in agricultural soils was 3.3 mg/kg [15,16]. Elevated levels of Cd were also found in rhizosphere soil in cocoa crops in Colombia, with median values of total Cd up to 1.86 mg/kg [17]. Cd contamination was reported in cocoa farming systems in Africa, Asia, Central America, and South America [18–20]. In France, simulations predicted that the continued use of phosphate fertilizers would increase Cd content in agricultural soils by 15 % over the next century [21]. Comparative risk assessment showed that Cd accumulation is higher in rice and wheat than in maize, making these staple crops particularly susceptible to contamination. However, the risk associated with maize cultivation also remained significant. Cd accumulation in this plant increased when it *co*-occurred with low-density polyethylene microplastics. Then, Cd content in shoots was higher by 25.5 % as well as in roots, by 9.1 %, which reduced the crop yield [22]. Due to the fact that Cd contamination of agricultural soils has reached alarming levels in so many regions, the development of remedial measures, such as materials capable of sorbing Cd, is urgent and of high importance.

So far, several remediation approaches have been explored, including phytoextraction [23], microbial remediation [24], and sorption [25–32]. Among these methods, sorption stands out as an efficient, low-cost, and versatile technique that is extensively studied for water and soil purification [25–32]. Adsorbents based on clay minerals [33–37] and polymers [37–51] proved a great affinity for Cd^{2+} ions and other toxic metals due to large surface area, high cation exchange capacity, and adaptability to various environmental conditions. Clays, such as natural MMT [33] and synthetic Lap [34], can bind heavy metals due to their layered structure and negative surface charge, based on ion exchange and surface complexation [33,34]. However, their application in practice is accompanied by some problems. Such solids usually form stable colloidal suspensions, making their separation from aqueous systems extremely labour-intensive [38]. On the other hand, polymer-based sorbents offer great design flexibility and reusability, enhancing their suitability for practical applications [39–52].

Composite materials combining polymeric and inorganic species have been increasingly studied and applied [53–67]. These materials can demonstrate better performance in terms of sorption kinetics, capacity, and reusability than individual components [56]. Composites based on alginate (Alg) seem to be particularly promising due to carboxyl and hydroxyl groups able to interact with pollutants, namely heavy metals and dyes, based on ion exchange or complexation [52–55,58,63,67–73]. Furthermore, these materials can form strong three-dimensional hydrogel systems by ionic cross-linking, characterized by high mechanical resistance, water retention, and stability [74]. Alg-based HGs cross-linked with Ca^{2+} exhibit unique swelling characteristics due to the formation of two-dimensional structure known as the "egg-box" model, in which Ca^{2+} interacts with the guluronic acid units of Alg to create a stable gel network. But, the obtained gels have insufficient mechanical properties, elasticity as well as high stiffness, and fragility. Incorporation of clay fillers can be applied to overcome these limitations. Alg-clay nanocomposites, such as Alg/bentonite, Alg/MMT, and Alg/kaolin, offer high efficiency in removal of toxic heavy metals like Cu(II), Pb(II), Cd(II), and Ni(II) from water [58–61,65,68,69,75–80]. They can also bind uranium [68], which makes them versatile, cost-effective sorbents for diverse environmental applications. Previous studies confirmed that MMT and Lap incorporation into hydrogels caused a significant increase in sorption of Cr(VI), Cr (III), and Pd(II) [65–67]. Besides good sorption capacity, the prepared composites revealed improved structural stability, reproducibility after several cycles of use, and better selectivity to heavy metal ions in multicomponent systems.

Considering the great sorption capacity of individual components towards Cd ions as well as the benefits of composite HGs described in the literature and our previous results, the current study aimed at developing highly efficient sorbents of Cd^{2+} ions based on Alg, filled with nanoclays – MMT and Lap. Investigating mechanisms of water/heavy metal sorption, we focused on the effects of filler content and type as well as cross-linker concentration on sorption properties and physicochemical advantages of the final products. Such development offers new solutions for removing Cd^{2+} ions from contaminated waters and soils, with significant implications for environmental management and sustainable agriculture. Alginate is a biocompatible, biodegradable, and cost-effective biopolymer, whereas nanoclays are easily available and cheap solids, with a well-developed structure and many functional groups. This makes them highly desirable in the synthesis of adsorbents and soil additives. The approach, in which the effects of fillers and cross-linker concentrations are studied in such detail, is not popular. Additionally, the relationship between sorption of water and sorption of heavy metal ions in the virtually entire pH range is rarely studied. All these aspects were described in this paper, which allowed for effective regulation of synthesis conditions and optimization of HGs composition. The biosafety tests of the composites are also not performed often, but their results are extremely important for the widespread use of all materials in the environment. Thus, exactly these analyses were conducted within this study and the obtained results allowed to conclude about real impact of the developed HGs on organisms.

2. Materials and methods

2.1. Materials

Alginic acid sodium salt (>99.0 %, viscosity (1 % in water): 450–550 cP, molecular weight: 300–500 kDa, Glentham Life Sciences, United Kingdom) was chosen as a biopolymer for the creation of composite HGs. Calcium chloride anhydrous ($CaCl_2$, pure p.a, Chempur, Poland) was used as a cross-linking agent, whereas montmorillonite (K10, powder, Sigma-Aldrich) and Laponite RD (Pulver, Kremer Pigmente GmbH&Co.KG, Germany) were applied as fillers. Cadmium(II) chloride ($CdCl_2$, 99 %, for analysis, anhydrous, Acros Organics, Belgium) was used as a source of heavy metal ions.

2.2. Characterization techniques

2.2.1. Scanning electron microscopy (SEM)

Morphological and elemental analyses of the samples were made using a MIRA3 LMU high-resolution scanning electron microscope (TESCAN GROUP) equipped with Oxford X-Max 80 energy-dispersive X-ray spectroscopy system. The samples sprayed with a conductive Au layer at an accelerating voltage of 10 kV were investigated.

2.2.2. X-ray diffraction (XRD)

Phase compositions of the solids were characterized by X-ray diffraction on a Panalytical XPert Pro MPD. A copper lamp (CuKα = 1.54178 Å) was used as the emission source. The test was carried out in the angular range of 2–65° 2θ with a step equal to 0.02° 2θ lasting 5 s. The X'Pert Highscore software was used to process the diffraction data.

2.2.3. Fourier transform infrared (FTIR) spectroscopy

FTIR spectra of the samples were registered in the range of 4000–400 cm^{-1} on a ThermoNicolet iS10 FTIR spectrometer equipped with ATR attachment with a diamond crystal.

2.3. Synthesis of the composite HGs

Alginate-based hydrogels (Alg-HGs) were prepared through ionic cross-linking using calcium chloride as a cross-linker. In the initial phase, a solution of sodium alginate (Na-Alg) was prepared by combining it with MMT or Lap clay. A necessary quantity of the filler (0–10 g) was thoroughly mixed with 10 g of Na-Alg. The resulting mixture was added in portions to 500 mL of distilled water and dissolved with continuous stirring and heating (up to 40–50 °C) until the Na-Alg was completely dissolved within 3–5 h. Next, 1000 ml of a cross-linker ($CaCl_2$) solution with a concentration of 0.25–2 wt% was prepared. Then, previously prepared 500 mL of Na-Alg/clay mixture was gradually introduced into the cross-linker solution using a syringe. The resulting mixture was kept for 1 h at room temperature. At the next stage, the synthesized HGs were washed 3 times with distilled water (to remove residual cross-linking agent), transferred onto a tray, and dried in an oven at a 50 °C for 2–3 days and at room temperature until being completely dry. Finally, the resulting samples were crushed using a grinder to obtain particles of about 1–3 mm in size. The composition and labelling of the composites are given in Table S1. The prepared composite HGs were labelled as: Alg/20%MMT, Alg/20%Lap, Alg/33.3% MMT, Alg/33.3%Lap, Alg/50%MMT, Alg/50%Lap, according to the amount (20–50 %) and type of nanoclay (MMT or Lap). The hydrogel without filler was marked as Alg.

2.4. Swelling studies

Swelling was tested applying the weight method at room temperature (22 °C) by determining the mass of the swollen gels depending on the time of their exposure to water. To conduct the experiment, the sample of dried hydrogel (0.015–0.02 g) weighed with an accuracy of 4 digits was placed in a glass jar, and 10 mL of distilled water was added and left to swell. At the controlled intervals, the HG sample was filtered using a fine sieve, and residual moisture was carefully removed with a lint-free paper filter. In the next step, the HG sample was weighed. Then it was put back into the jar with 10 mL of distilled water for further swelling, after which the experiment was repeated until an equilibrium state was reached (when the mass of the sample remained stable). To study the kinetics of swelling and the mechanism of solvent diffusion into HGs, all experiments were conducted at least three times. The experimental data were presented as the mean values, with the standard deviations not exceeding 10 % of their mean values in all tests.

The swelling degree Q was determined gravimetrically according to the formula [81]:

$$Q = \frac{(w_t - w_0)}{w_0} \tag{1}$$

$$Q_\infty = \frac{(w_{eq} - w_0)}{w_0} \tag{2}$$

where w_0 is the weight of a dried hydrogel, w_t is its weight at the swelling time t, and w_∞ is the weight of a completely swollen hydrogel at an equilibrium state.

To analyze the effect of clay content on the swelling behaviour of composite HGs, they were immersed in distilled water at pH 6.5–7.0. Swelling tests of Alg, Alg/50%MMT, and Alg/50%Lap synthesized using 0.3 wt% $CaCl_2$ were carried out in the pH range of 2–11. The pH value of HG solutions was adjusted by adding a small amount of 0.1 M or 1 M HCl or KOH. The samples were kept under constant stirring in the solutions with appropriate pH at room temperature, for 24 h, until swelling equilibrium was established.

To evaluate the mechanism of water diffusion in the synthesized HGs, according to the Korsmeyer-Peppas model, the following equation was used:

$$F = \frac{M_t}{M_\infty} = kt^n \tag{3}$$

where F denotes the amount of solvent fraction at time t; M_t and M_∞ correspond to the amount of solvent diffused into the gel at time t and at time ∞ (in the equilibrium state) respectively; k is the constant associated with the structure of the HG network; the swelling exponent n is the number that determines the type of diffusion [82].

2.5. Potentiometric titration

The variable surface charge (Q_{var}) of the tested HGs synthesized using 0.3 wt% $CaCl_2$ was determined by potentiometric titration. This charge is derived from the dissociation and association of H^+ ions present on the surface of the studied material.

In the titration process, the addition of hydroxyl ions (OH^-) neutralizes the protons (H^+) of the acidic functional groups present on the surface of the tested material. As a result, there is an increase in the negative surface charge. The obtained curves represent the variation of surface charge occurring in the solid phase ΔQ_v, depending on pH:

$$\Delta Q_v = N_{sus} - N_{sol} \tag{4}$$

where: N_{sus} – the amount of base consumed during titration (mol), N_{sol} – the number of moles of base consumed during titration of the equilibrium solution [83,84].

Cation exchange capacity (CEC) was estimated as the number of moles of base consumed during titration to pH 7 [85]. Higher CEC values indicate a stronger interaction between the adsorbent and the adsorbate [86].

The assumption that the surface activity of protons is equal to their activity in solution and the total number of functional groups corresponds to the maximum increase in the variable charge was used to determine the fractions of surface functional groups relative to the apparent surface dissociation constant, pK_{app}:

$$f_i\left(pK_{app,i}\right) = \frac{\frac{1}{Q_{max}\left|\Delta SO^-(pH_{i+1}) - \Delta SO^-(pH_i)\right|}}{\left(pK_{app,i+1} - pK_{app,i}\right)} \tag{5}$$

where: $pK_{app,i}$ is the pH value, Q_{max} is the maximum increase in the surface charge, and SO^- is the amount of surface charge that comes from the dissociation of surface functional groups at a given pH.

The average value of pK_{app} ($pK_{app,av}$) was calculated as:

$$pK_{app,av} = \sum_{i=1}^{n} pK_{app,i}\, f_i\, pK_{app} \tag{6}$$

Strongly acidic groups, i.e., carboxylic ones, are characterized by low pK_{app} value (about 3.2), which means that they may dissociate at low pH values. Lactonic groups are of medium pK_{app} value (about 5.7), whereas phenolic ones – of high pK_{app} value (about 9.7). The titration was performed in the pH range from 3 to 10. As the pH increases, the charge becomes greater, due to the deprotonation of the surface functional groups.

2.6. Sorption experiment

A series of tests was carried out to examine parameters influencing the sorption of Cd^{2+} ions, including contact time, pH, adsorbent quantity, and initial adsorbate concentration.

The sorption isotherms were determined for the initial concentrations of 50–1000 mg/L. The samples were prepared using 20.0 mg of the solid and 20 mL of the $CdCl_2$ solution, and pH value was adjusted to 6.5–7.0 for all systems. The sorption process was conducted at 22 °C, for 48 h to establish equilibrium, under shaking conditions (30 rpm, Rotator Multi RS-60, Biosan, Poland). After its completion, HG particles were

separated by centrifugation (1000 rpm, 10 min, SBS-LZ-4000/20–6, Steinberg Systems). The Cd^{2+} ions concentration was determined in the obtained supernatants by ion-selective electrode (S.A. Electrochemical Equipment detector) connected with pH/Ion METER SPI-505 (ELMETRON, Poland).

Kinetic sorption experiments were conducted for initial Cd^{2+} ions concentration of 200 mg/L. 1.0 g of the solid was immersed in 500 ml of the Cd^{2+} ions solution and agitated at 800 rpm with magnetic stirrer (SBS-MR-1600/6, Steinberg Systems). At specified intervals, 5 mL of the analyzed solution was extracted, and the Cd^{2+} ions concentration was quantified using the method described above. To study the effect of pH value, sodium hydroxide (0.01 and 0.1 M) or hydrochloric acid (0.01 and 0.1 M) were used to adjust the pH of the reaction mixture.

The sorbed amounts of Cd^{2+} ions (mmol/g) determined per unit mass of the dry sorbent at time t (q_t) (7) and at the equilibrium (q_e) (8) were calculated according to the equations:

$$q_t = \frac{(C_0 - C_t)V}{m} \tag{7}$$

$$q_e = \frac{(C_0 - C_e)V}{m} \tag{8}$$

where C_0, C_t, and C_e are the initial, the final at time t, and at the equilibrium concentrations of Cd^{2+} ions in the solution (mmol/L); V is the volume of the tested solution (L); m is the mass of the dry sorbent (g).

The removal efficiency (R, %) was calculated as follows:

$$R = \frac{C_0 - C_e}{C_0} 100\% \tag{9}$$

Two most frequently used isotherm models, of Langmuir and Freundlich, as well as two kinetics equations, pseudo-I- and pseudo-II-order ones [87–89], were chosen to model experimental data. Each experiment was conducted three times and the mean values were presented on the charts.

2.7. Biosafety testing

The genotoxicity and cytotoxicity of HGs were investigated using the mouse fibroblast cell culture L-929 (ATCC: CCL-1™), a classic model for in vitro studies. DMEM/F12 cell culture medium, fetal bovine serum, antimycotic antibiotic, trypsin-EDTA solution, DMSO, crystal violet, and thiazolyl blue tetrazolium bromide (MTT) were used to treat L-929 cell culture. To obtain the medium of HG and conditioned culture, the HG samples were placed in Dulbecco's phosphate-buffered saline (DPBS, Sigma, USA), and 10 wt% HG in DPBS was prepared. Then, the cytotoxicity and genotoxicity of 1 wt% HGs in the culture medium were investigated. The cytotoxicity was determined after 24 h of exposure of L-929 cell culture to HG. The results were expressed as a percentage of the number of metabolically active and adherent intact cells cultured under the identical conditions in the 96-well plates simultaneously.

To determine the cell viability after their contact with HGs, two key indicators were tested: metabolic activity (MTT test) and total number of adherent cells (crystal violet (CV) test) [90–92]. These tests are based on the optical density of the wells with cells after their treatment with appropriate reagents/dyes. The number of living cells (N) for both methods was calculated according to:

$$N = \frac{OD_{exp}}{OD_{cont}} 100\% \tag{10}$$

where OD_{exp} is the optical density of the solution in the experimental wells; OD_{cont} is the optical density of the solution in the wells of the intact control.

The optical density was measured using a Multi scan Ascent vertical beam spectrophotometer (Thermo Labsystems, Finland) at a wavelength giving the maximum absorption of selected dye. A DPBS solution, which was also introduced into the cell monolayer with subsequent double titration in the cell culture medium, was used as a control. That is why, the indicators of two controls were taken into account during the result analyses: (1) the control of intact cells, (2) the control of the effect on metabolic activity and the total percentage of adherent cells of the DPBS control. The study of data and parameters was statistically processed and presented as the median with the interquartile range Me (LQ-UQ), where Me = median (50 % percentile), LQ = 25 % percentile, and UQ = 75 % percentile. Statistical calculations were performed using the Stat Plus Pro 5.9.8 software and STATISTICA *v*.10 (Experimental Data Analysis System, StatSoft, Inc. 2011).

The genotoxicity of experimental HG was assessed in vitro by the DNA-comet method under alkaline conditions according to the described technique [93–95]. The genotoxic effect of 1 wt% HG in conditioned DPBS was analyzed.

3. Results and discussion

3.1. Material characterization

3.1.1. Structural characteristics of composite HGs

The analyses of morphology and elemental composition indicated that, at larger magnification, spherical particles with a diameter in the range of 30–50 nm can be distinguished in the MMT samples (Fig. 1a). They overlap each other, forming a flocculent, hierarchical, layered structure with pronounced spaces between its layers. The sizes of the observed aggregates were mainly from 0.2 to several μm and were not ordered in space (Fig. 1b). The EDX analysis indicated that mineral phase of MMT had the following composition: O – 62.7 at.%, Si – 24.5 at.%, Al – 5.7 at.%, Fe – 1.54 at.%, Mg – 0.69 at.%, and K – 0.74 at.%, which corresponded to the stoichiometric formula of K-MMT – $K_{0.03}(Mg_{0.03}Al_{0.24}Fe_{0.05})Si_4O_{10}(OH)_2$.

The SEM micrographs (Fig. 1c) of Lap indicated that it consisted of clearly visible spherical particles with the diameters of 10–30 nm [96]. Such particles interacted with each other to form large, densely packed, irregularly shaped aggregates observed at smaller magnification (Fig. 1d). According to EDX analysis, the main elemental components of Lap were as follows: O – 62.4 at.%, Si – 20.3 at.%, Mg – 15.3 at.%, and Na – 1.9 at.%, (Table S2), which was consistent with the stoichiometric formula $Na_{0.75}(Si_8Mg_6Li_{0.3})O_{20}(OH)_4$ [38]. The cross-section images of cross-linked Alg showed formation of a continuous homogeneous network (Fig. 1f), while those recorded at large magnification (Fig. 1e), formation of an interpenetrating polymer layer with a uniform structure, apparently arising from the removal of solvent during the HG drying.

The Alg/MMT images revealed a homogeneous MMT distribution throughout the Alg matrix with a tendency to form a layered structure. Small magnification images (Fig. 1h) showed evidently two separate phases of polymer and MMT. However, the MMT phase in the composite HGs appeared with a looser framework and larger internal channels between the platelets compared to the initial clay (Fig. 1 gh). Such a change can be due to the physical intermolecular interaction between the Alg and the filler, which led to the formation of a mixed intercalation-flocculation structure in the polysaccharide matrix. The Alg/Lap images demonstrated formation of homogeneous and stable network of uniformly distributed nanoclay particles, which were arranged in some chain structures (Fig. 1 ij). It has been reported that polymers can be easily adsorbed on the nanoclay surface due to specific interactions, such as electrostatic, ionic interactions, hydrogen bonds [97], or even hydrophobic interactions. Dispersion of Lap during composite HG formation can lead to disaggregation between stacked elementary disk crystals of nanoclay or a set of stacked disks. Then, a significantly larger surface area of nanoclay becomes available for the polymer chains [97].

The XRD analysis of Lap (Fig. 2c,d) showed characteristic reflections at $2\theta \approx 6.4°$, corresponding to a d-spacing of ~13.8 Å, typical for layered silicates. The (001) basal reflection shifted to $2\theta \approx 6.0°$, 5.6°, and 5.5°

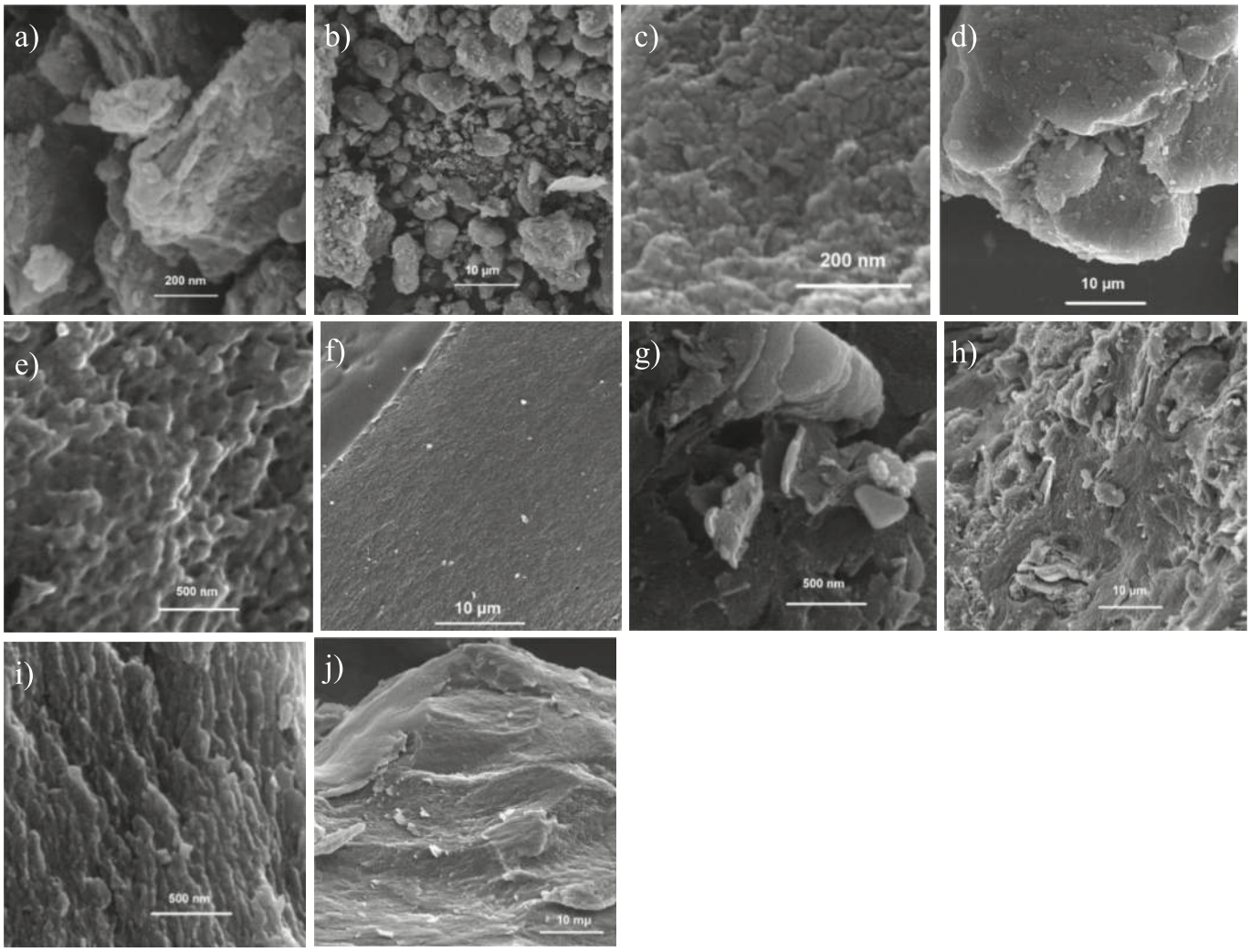

Fig. 1. SEM micrographs of MMT (a, b), Lap (c, d), cross-linked Alg (e, f), and composite HGs: Alg/MMT (g, h), Alg/Lap (i, j).

for Alg/50%Lap, Alg/33.3%Lap, and Alg/20%Lap, respectively, that indicated an expanded interlayer spacing of ~14.7 Å, ~15.8 Å, ~16.1 Å, suggesting Alg intercalation between Lap layers [98]. The XRD analysis of MMT (Fig. 2a,b) presented a (001) reflection at $2\theta \approx 5.9^{\circ}$, corresponding to a 14.9 Å interlayer spacing, confirming its pre-treated structure. This reflection shifted to 6.0–6.3° (~14.7–14.0 Å) for Alg/MMT, indicating a mixed intercalated/flocculated structure with partial disorder. For the unfilled Alg gel, broad halo was observed in this region (Fig. 2a), indicating amorphous structure. The reflections at 31.86°, 45.53°, and 56.37° most likely corresponded to sodium chloride released during the cross-linking process. Thus, there was a clear difference in the distribution of MMT and Lap in the alginate matrix. In Alg/Lap, an increase in the interlayer distance was notices, which confirmed the effective penetration of Alg into the layered structure of Lap. For Alg/MMT, the interlayer space decreased, indicating a possible aggregation or sticking of MMT particles instead of complete intercalation of the polymer.

Other XRD patterns characteristic of Lap [99] and MMT [100] in the composite HGs remained unchanged, indicating that the original crystal structure of nanoclays was preserved and their integration with the Alg matrix did not lead to any structural changes.

3.1.2. *FTIR spectra of Alg-based HGs filled with nanoclays*

The FTIR analysis was used to investigate potential interactions between the HGs components. Fig. 3 presents the FTIR spectra of Alg, MMT, Lap, as well as the composite HGs.

The spectrum of cross-linked Alg showed characteristic peaks of symmetric and asymmetric stretching vibrations of carboxyl groups (–COO) at 1415 and 1589 cm^{-1}, respectively, as well as the peak with at 1025 cm^{-1} corresponding to the C—O stretching vibration in the polysaccharide structure. The peak at 2928 cm^{-1} represented stretching vibrations of aliphatic C—H bonds, and the broad peak at 3247 cm^{-1}, stretching vibrations of hydroxyl groups (–OH). The MMT spectrum showed: characteristic peaks at 1017 cm^{-1} corresponding to the stretching of the Si—O bond in the plane, the peaks around 797 cm^{-1} attributed to the bending of Si—O in SiO_2, the shoulder at 923 cm^{-1} corresponding to the bending vibrations of Al–OH, and the peak at 521 cm^{-1} attributed to the bending vibrations of the Al–O–Si bond. The bands at 3618 cm^{-1} indicated the presence of hydroxyl groups on the surface (Si–OH and Al–OH stretching) and those around 3392 cm^{-1}, the stretching of structural hydroxyl groups and water. Furthermore, the band at 1628 cm^{-1} in the spectrum indicated water deformation [101].

In Alg/MMT, an increase in MMT content resulted in a steady displacement of the band at 1595 cm^{-1} to higher wavenumbers, indicating interactions between carboxyl groups of the polymer and hydroxyl groups located on the surface of MMT platelets. Formation of hydrogen bonds between the silanol groups of MMT and Alg carboxyl groups was also confirmed by the Si–OH stretching of MMT at 3618 cm^{-1}, which disappeared in the Alg/MMT [102]. A broad band of Si—O at 1014 cm^{-1} in the MMT spectrum is sensitive to intercalation. Thus, its

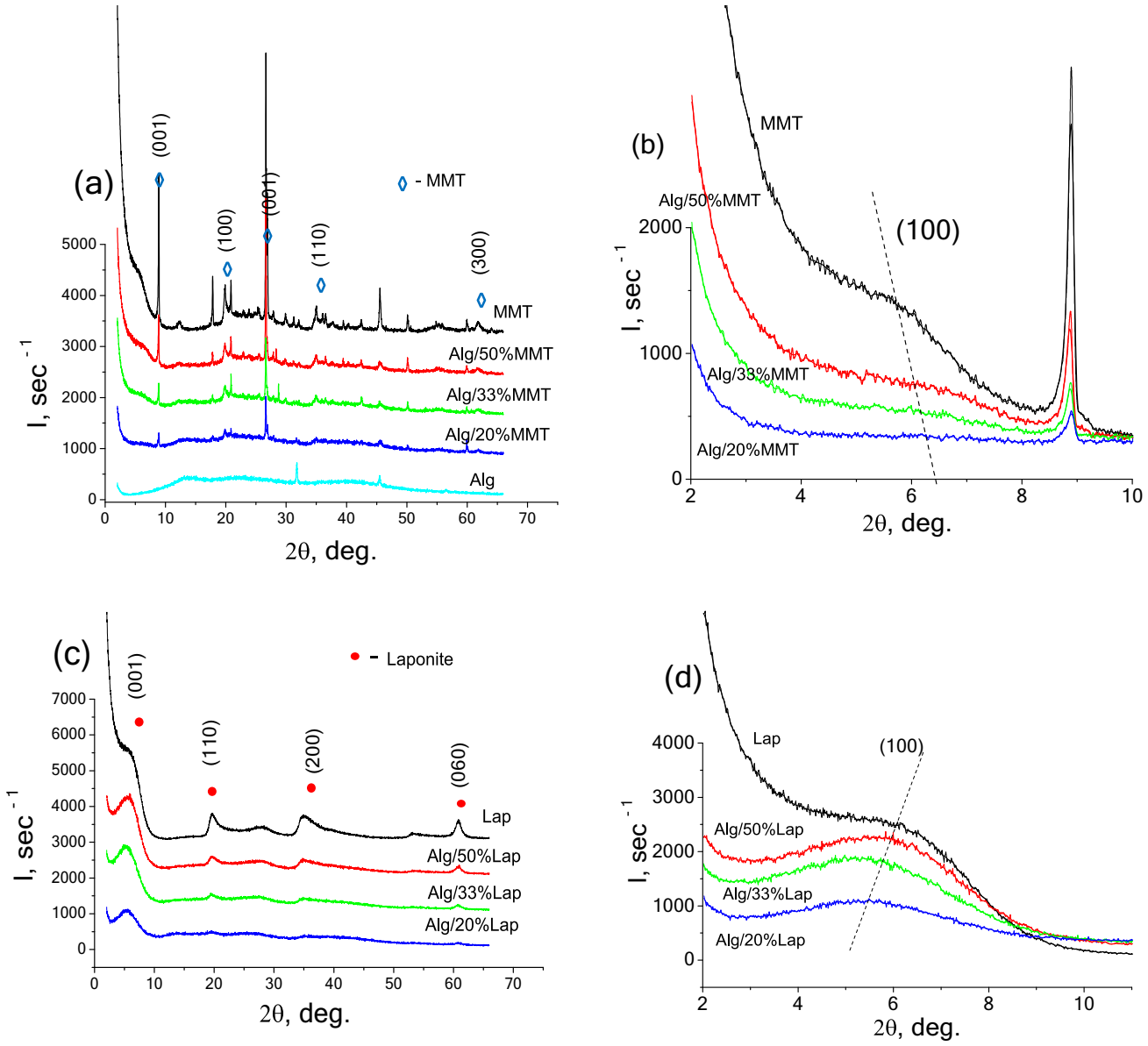

Fig. 2. XRD patterns for MMT (a), Lap (b) and composite HGs (a-d) synthesized using different component ratios.

slight shift to 1020–1025 cm^{-1} for MMT-filled composite HGs can indicate an increase in interlayer distance and intercalated structure formation.

The main characteristic bands for Lap were attributed to the stretching vibrations of Si—O (at 969 cm^{-1}), to the Mg–OH–Mg bending vibrations (at 652 cm^{-1}), and the Si–O–Mg deformation vibrations (at 435 cm^{-1}) [103]. The spectrum contained also bands of surface hydroxyl groups (–OH stretching) and physically sorbed water at 3700–3000 cm^{-1}, as well as deformation of hydroxyl groups at 1630 cm^{-1} (–OH bending) [96].

A shift of the band of the stretching vibrations of Si—O bonds towards lower wavenumbers was observed for Alg/Lap (e.g., for Alg/20% Lap, this band was recorded at 997 cm^{-1}). This was caused by the interaction between clay and polymer [104]. In addition, for Alg/50% MMT and Alg/50%Lap, a band corresponding to asymmetric –COO stretching was shifted from 1589 to 1596 cm^{-1} (compared to unfilled Alg). This phenomenon is characteristic for the HG cross-linking through physical interactions and can be associated with additional electrostatic interaction between polymer carboxyl groups and nanoclay hydroxyl ones [105].

3.2. Study of swelling properties

3.2.1. Effect of cross-linking agent concentration and clay filler content on swelling

The results of the swelling kinetics of Alg, Alg/MMT, and Alg/Lap are shown in Fig. 4 and S2. Fig. S3 shows also the equilibrium swelling degrees (Q_∞) for the investigated materials calculated using Eq. (2).

The most intensive water uptake occurred during the first 4–6 h, and this process continued mainly up to 24 h for most samples (Fig. 4a). The largest swelling degree (Q) was noted for Alg synthesized using 0.25 wt % C_{CaCl2}–120 mg/g after 24 h. However, for this sample, 144 h, the gradual increase in the Q value occurred, reaching 135 g/g, and it did not hold its shape well and had a visibly unstable structure. Such gels destroyed under pressure with simultaneous release of water from them, which can be elucidated by insufficient formation of cross-linking bridges for this $CaCl_2$ concentration. In the C_{CaCl2} range of 0.25–0.5 wt%, a nonlinear dependence of the degree of cross-linking on C_{CaCl2} was revealed for Alg, Alg/MMT, and Alg/Lap. Increasing C_{CaCl2} to 0.3 wt % resulted in the formation of stable unfilled Alg, which did not change its mass after 24 h of exposure to water. But, the obtained HG was

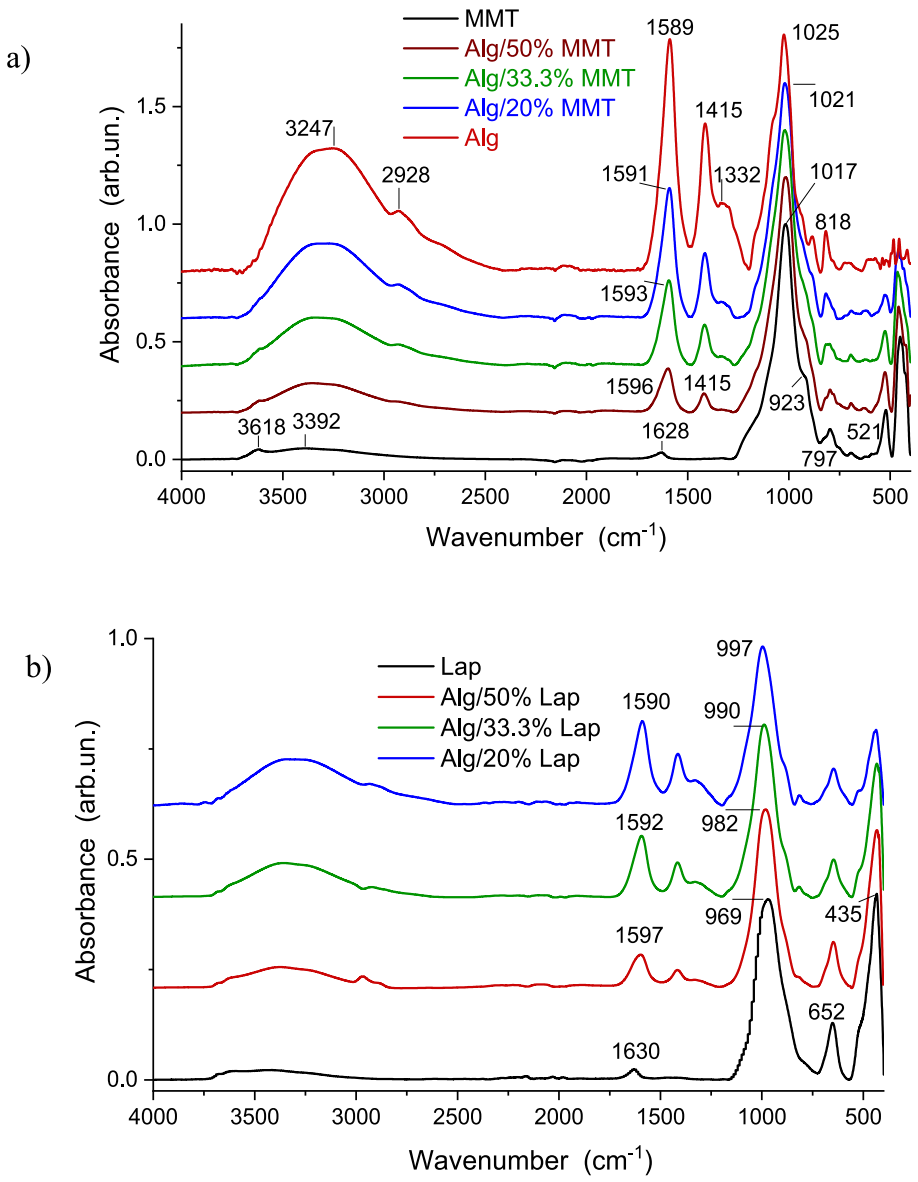

Fig. 3. FTIR spectra of MMT and Lap as well as composite HGs with different content of MMT (a) and Lap (b).

characterized by the Q_∞ value equal to 74 g/g.

The Q_∞ parameters depended on the cross-linker concentration used for the synthesis and the filler content (Fig. S2). All composites with MMT, synthesized at C_{CaCl2} of 0.25 wt%, were stable during exposure to water and were not crushed under slight pressure. The Q_∞ values for the Alg/20%MMT, Alg/33.3%MMT, and Alg/50%MMT (0.25 wt% $CaCl_2$) were 102 g/g, 67.6 g/g, and 53.5 g/g, respectively. This indicated that clay nanoparticles can act as additional cross-linking elements for Alg macromolecules [102]. A different situation was noticed for HGs with Lap, prepared using C_{CaCl2} of 0.25 wt%. For these samples, an increase in swelling occurred during the first 6 h, followed by a decrease (Fig. S1). A clearly expressed so-called overshooting effect was observed, which can be explained by the relaxation and rearrangement of polymer chains or formation of additional chemical or physical cross-links [106]. Furthermore, these samples (prepared using C_{CaCl2} of 0.25 wt%) exhibited instability and dissolved upon prolonged exposure to water. At the same time, after swelling Alg/20%Lap, Alg/33.3%Lap, and Alg/50% Lap prepared with 0.3 wt% $CaCl_2$, elastic, stiff samples were obtained, which retained their shape well and did not collapse under moderate pressure even after long-term exposure to water for 192 h. The Q_∞ parameter for these samples was 73.4 g/g, 61.6 g/g, and 52.8 g/g, respectively.

The results showed that the Q value of HGs with MMT (at 0.3 wt% $CaCl_2$) was smaller compared to that for HGs with Lap. This could indicate a more pronounced cross-linking effect of MMT compared to Lap. The Q_∞ for the Alg/20%MMT, Alg/33.3 % MMT, and Alg/50 % MMT (at 0.3 wt% $CaCl_2$) was 66.2 g/g, 50.1 g/g, and 37.6 g/g, respectively. Low Ca^{2+} concentrations resulted in the formation of a weakly cross-linked network, providing larger swelling. In turn, elevated C_{CaCl2} contributed to a more compact cross-linked network, diminishing the swelling capacity of HGs [107]. By C_{CaCl2} increasing there were obtained stable HGs capable of absorbing and retaining water in their structure without being destroyed or dissolved in water under the experimental conditions. But, a significant decrease in the Q_∞ value was observed then, especially for C_{CaCl2} above 0.5 wt%. The reduction in the Alg/MMT and Alg/Lap swelling could be due to the nanoclays occupying voids within the HG matrix, diminishing the water molecules infiltrating [106]. In addition, the Alg content per unit dry mass decreased in the Alg/MMT and Alg/Lap.

To sum up, C_{CaCl2} below 0.25 wt% was insufficient to form a strong and stable HG network for Alg and Alg/Lap. However, the Alg/MMT samples proved to be more stable under these conditions, which can be

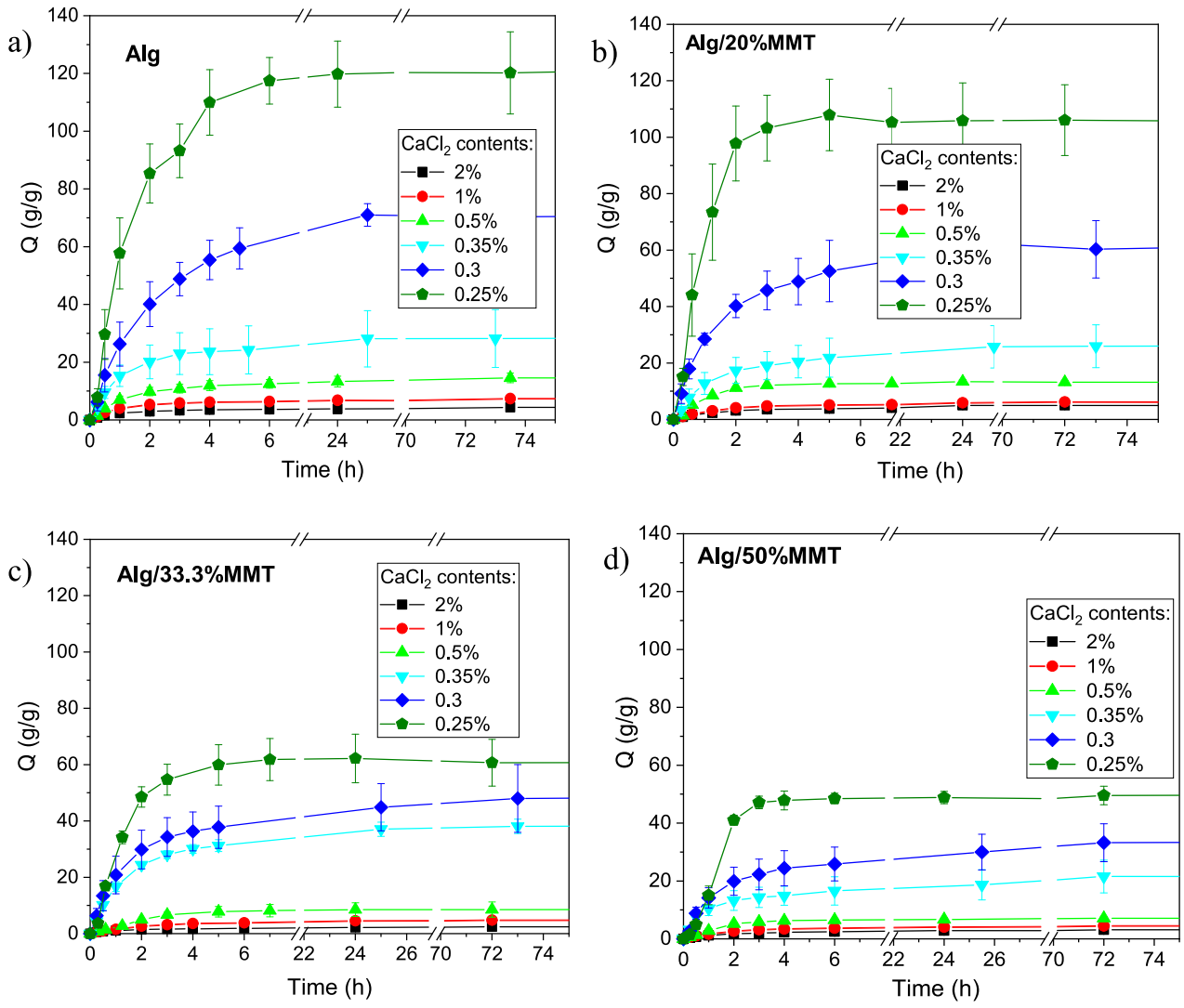

Fig. 4. Dependence of the swelling ratio (*Q*) on time of exposure in water for Alg (a) and Alg/20%MMT (b), Alg/33.3%MMT (c), and Alg/50%MMT (d) synthesized using different concentrations of the cross-linking agent ($CaCl_2$).

explained by additional cross-linking properties of this clay. C_{CaCl2} above 0.5 wt% led to a significant drop in the swelling degree of the studied materials.

3.2.2. Swelling kinetics

The swelling degree of Alg-based HGs was provided by the balance between the osmotic pressure driving water into the gel and the elastic forces of the formed network preventing further expansion. HGs typically reach an equilibrium swelling state when these forces are balanced [82,108]. According to Siepman and Pepas [109], by defining the diffusion exponent *n* in Eq. (3), it is possible to obtain information about the physical mechanism that controls the absorption or release of a solute. Depending on the geometric shape of the gel samples, a release exponent *n* smaller than 0.5 corresponds to the pseudo-Fickian diffusion [110]. When *n* is equal to 0.5 diffusion (Fickian) mechanism (Case I) is observed. While $n = 1$, Case II transport (zero-order release) is found. Case III diffusion takes place when $0.5 < n < 1$, which is also called anomalous or non-Fickian. Finally, Super Case II transport is noted at $n > 1$. These values for the swelling exponent *n* for spherical particles are given in [111]. The differences between these mechanisms are detailed in SI.

Eq. (3) was used to determine the nature of the water diffusion into Alg-based HGs with and without nanoclays. It should be noted that Eq. (3) is valid for the initial stages of swelling (first 60 % of the normalized water uptake) [112]. Kinetic curves for unfilled Alg are presented in Fig. 4a. The corresponding plots of $\ln(M_t/M_\infty)$ vs $\ln(t)$ for Alg can be found in Fig. S4a. whereas those for Alg/Lap at different C_{CaCl2}, in Fig. S4b. The exponents *n* and constants *k* values were calculated from the slope and intercept of the lines, respectively, and are presented in Table S3. It is worth noting that the vast majority of the results are statistically significant, as $R^2 \gg 0.95$. Analyzing the swelling kinetics of Alg/Lap using the Peppas-Korsmeyer theory (Table S3), it can be concluded that cross-linking agent concentration should be considered as determining factor in the swelling mechanism. Thus, at high C_{CaCl2} (0.5–2 wt%), true Fickian and pseudo-Fickian diffusion (which differs from Fickian diffusion by some slowdown in the final equilibrium state [113]) will be observed. In both cases the diffusion rate is much lower than the relaxation rate. The gel cross-linked to a small extent will absorb water following the Case II transport or Super Case II transport mechanism, where diffusion is very fast compared to the polymer relaxation process. In all intermediate cases, anomalous Non-Fickian diffusion takes place. Similar regularities were found for Alg/MMT, with decreasing cross-linking frequency transition from true Fickian diffusion to transport controlled by relaxation. The calculated swelling exponent values (*n*) were over 1 at 0.25 wt% of $CaCl_2$, 0.5–0.9 at 0.3–1 wt% of $CaCl_2$, and 0.2–0.4 at 2 wt% of $CaCl_2$.

3.2.3. Effect of pH on swelling

Swelling behaviour can be affected by environmental factors such as pH, ionic strength, etc. The pH changes can alter ionization state of Alg, affecting its interaction with Ca^{2+} ions and thus its swelling properties [81]. The studied HGs displayed significant pH sensitivity, showing enhanced swelling, particularly in neutral and alkaline environments (Fig. 5a). When the pH value is higher, a significant increase in the HGs volume was also observed (Fig. 5b-j).

As it can be seen in Fig. 5a, unfilled Alg showed the highest Q values in almost entire pH range. The composite HGs demonstrated smaller swelling degrees. Alg/50%MMT, exhibited the lowest *Q* values over the entire pH range. In the pH range of 6.5–8.5, the studied HGs demonstrated only slightly changing swelling degrees, which amounted to about 65, 48, and 33 g/g for Alg, Alg/50%Lap, and Alg/50%MMT, respectively. This was associated with complete dissociation of carboxyl groups of alginate [115].

A significant decrease in the swelling degree was observed for Alg and Alg/Lap at pH below dissociation constant (pK_a) of alginic acid, the value of which is in the range between $pK_a = 3.6$ for mannuronic acid and $pK_a = 3.8$ for guluronic acid [116]. At high H^+ concentrations, deionization of unbound carboxyl groups takes place and decrease in the electrostatic forces between polymer chains. The transition of ionotropic network to Alg-based HG structured by hydrogen bonds is also possible under these conditions [118]. For Alg/MMT, almost linear decrease in swelling degree was observed at pH below 6.5. Greater reduction in swelling for Alg/MMT, compared to Alg/Lap, can be explained by formation of additional hydrogen bonds between -OH groups of MMT and protonated -COOH groups of alginate [102,117]. At the lowest pH value (pH 2), all HGs demonstrated maximum cross-linking and the most compact structure.

Higher swelling degree of Alg/MMT and Alg/Lap was observed in alkaline pHs. At pH 11.4, Q_∞ can reach 44 g/g for Alg/MMT and 56 g/g for Alg/Lap. Then, HGs preserved their flexibility, remained unbroken, and did not degrade under mild stresses. In neutral and alkaline environments, Alg and MMT interacted based on electrostatic forces between $-COO^-$ groups of the polymer and positively charged edges of the clay plates [102].

3.3. Sorption studies

3.3.1. The removal efficiency of Cd(II) ions

The pollutant sorption depends on sorbent type and dose, pollutant nature, process conditions, etc. [116–126]. Fig. 6 presents the effect of initial Cd^{2+} ions concentration on the removal efficiency by Alg/MMT and Alg/Lap. A great efficiency was observed for low initial concentrations due to abundance of accessible active sites. At an initial concentration of 50 mg/L, the removal efficiency for Alg, Alg/50%MMT, and Alg/50%Lap, synthesized using C_{CaCl2} of 0.25 wt%, reached 97.3, 94.2, and 97.8 %, respectively. The obtained values are better than those of the most sorbents described in the literature (Table S4) [30,33,34,116–126]. Increasing initial concentration made sorption less efficient owing to the gradual filling of sorption sites.

The removal efficiency of Cd^{2+} ions by Alg, Alg/50%MMT, and Alg/50%Lap increased significantly with higher sample weight (20–50 mg) due to the greater availability of sorption sites, reaching 91.85 %, 87.9 %, and 93.1 %, respectively, for initial Cd^{2+} concentration of 200 mg/L

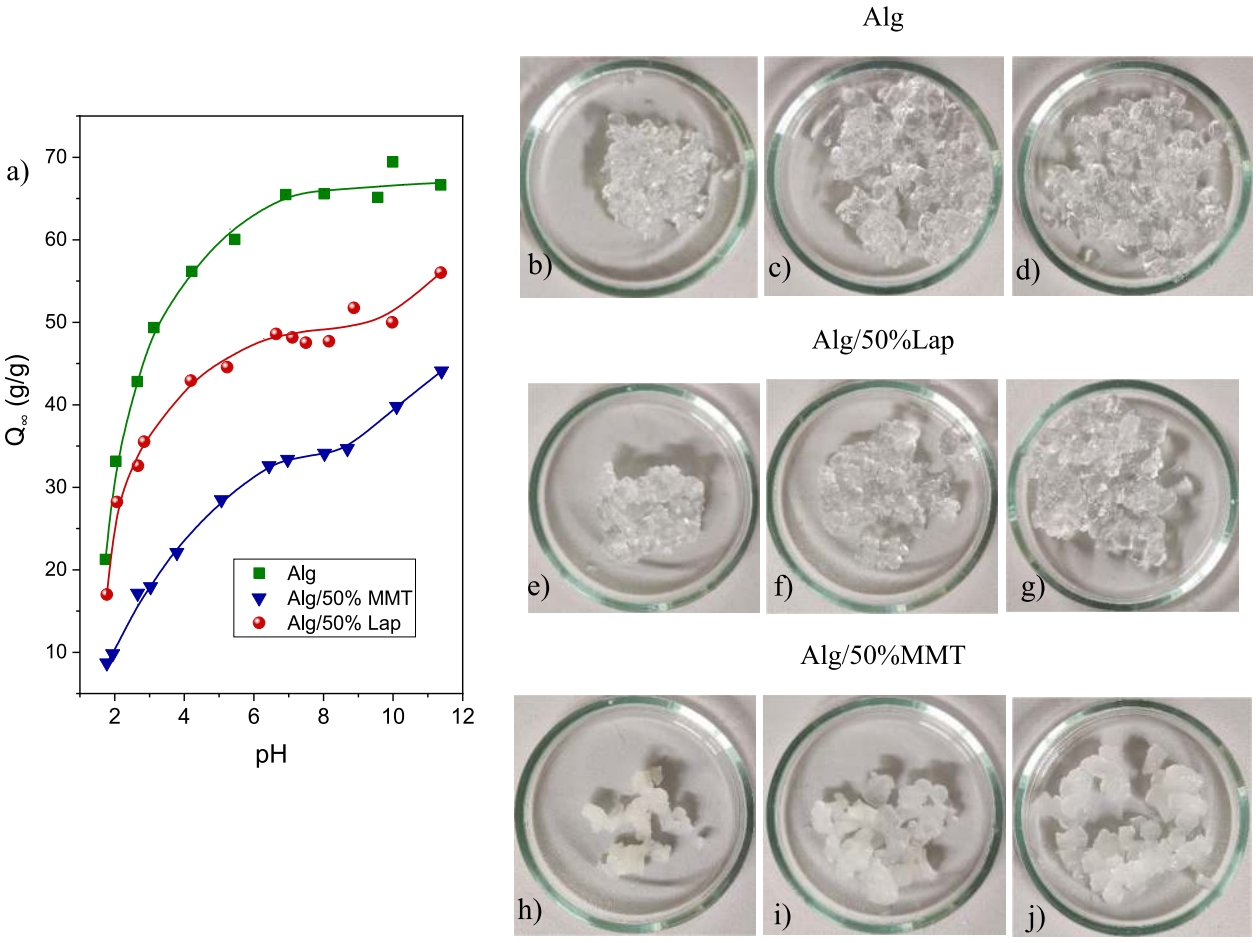

Fig. 5. Equilibrium swelling ratio (Q_∞) as a pH function for Alg, Alg/50%MMT, and Alg/50%Lap synthesized using C_{CaCl2} of 0.3 wt% (a) and photographs showing the comparative size of Alg (b, c, d), Alg/50%Lap (e, f, g), and Alg/50%MMT (h, i, j) after equilibrium swelling at pH 2, (b, e, h), pH 7 (c, f, i), and pH 11.4 (d, g, j).

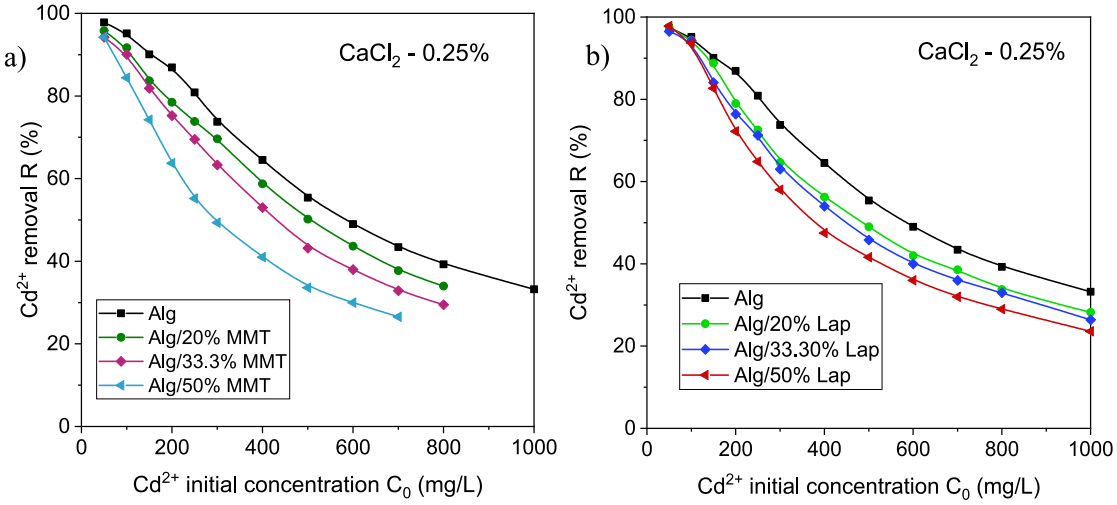

Fig. 6. Removal curves of Cd^{2+} ions for Alg, Alg/MMT, and Alg/Lap, prepared at C_{CaCl2} of 0.25 wt%, as a function of the initial Cd^{2+} ions concentration (initial pH value = 6.5, hydrogel dosages = 0.020 g, contact time = 48 h, solution temperature = 22 °C).

(Fig. S5a). However, the sorbed Cd^{2+} ions amount per unit mass decreased as solid content increased, likely due to competition among functional groups, reducing site availability per unit mass, although the maximum sorption capacity remained unchanged according to the Langmuir isotherm.

3.3.2. Sorption kinetics

The experimental data modeling showed that the pseudo-I-order model fitted the kinetics data in the initial (linear) portion of the kinetic curve. The obtained correlation coefficients (R^2) were 0.91 for Alg, 0.98 for Alg/MMT, and 0.95 for Alg/Lap (Fig. S6, Table S5). Nevertheless, the pseudo-II-order model fitted the experimental data for Alg, Alg/Lap, and Alg/MMT better than the physical sorption model. The R^2 values were >0.999 for all the samples. Thus, chemisorption was the rate-controlling step for Cd^{2+} ions in the tested systems. The applicability of both kinetics models for describing the Cd^{2+} ions sorption may indicate that both physical and chemical processes are included in this process. It was also noted that the k_1 and k_2 rate constants decreased for the composite HGs, compared to unfilled Alg, which was probably caused by the intraparticle-diffusion of Cd^{2+} ions into clay platelets. For

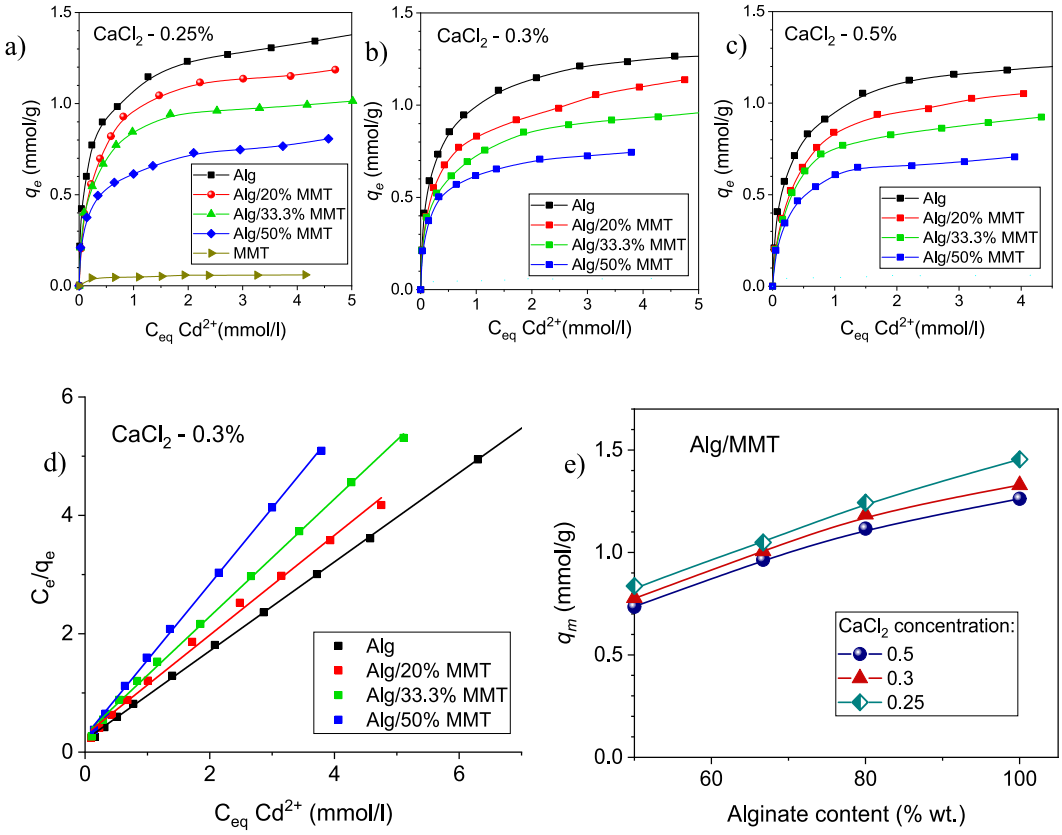

Fig. 7. Sorption isotherms of Cd^{2+} ions by Alg-based HGs filled with MMT prepared with C_{CaCl2} of 0.25 (a), 0.3 (b), and 0.5 wt% (c), Langmuir isotherms (d) and the value of maximum sorption capacity of Cd^{2+} ions as a function of the Alg content in Alg/MMT (e).

all HGs, the sorption equilibrium was reached after 6 h.

Other researchers also reported that adsorption kinetics for targeted contaminants (primarily fluoride) on their respective biopolymer-based composites followed pseudo-II-order models, indicating that chemisorption is the rate-limiting step [127–130]. They consistently observed rapid initial uptake within the first 30–60 min, achieving equilibrium thereafter. They used additionally intraparticle diffusion analyses, which showed a two-stage process: an early boundary-layer adsorption phase followed by slower intraparticle diffusion. The model of intraparticle diffusion also well described the experimental data obtained for the HGs studied in this paper ($R^2 = 0.999$).

3.3.3. Sorption isotherms

The sorption isotherms determined for HGs prepared using C_{CaCl2} of 0.25, 0.3, and 0.5 wt% are presented in Fig. 7 and S7. As mentioned previously, at low C_{eq} of Cd^{2+} ions, a significant increase in the amount of sorbed substance was observed since almost all metal ions could interact with active sorption centers on HGs, indicating a great affinity of the sorbate to the sorbent. With an increase in the equilibrium concentration, as the active sorption centers were filled, the maximum sorption capacity of the studied samples was achieved. The isotherms, which showed a rapid increase in the sorbed amount with the increasing concentration until reaching saturation, belonged to the type I isotherms in the IUPAC classification and was well described by the monolayer sorption model.

The parameters calculated using the Langmuir and Freundlich models are given in Table S6, whereas the sorption isotherms on the coordinates of the linear form of the Langmuir equation for Alg-based HGs filled with MMT and Lap, synthesized at C_{CaCl2} of 0.3 wt%, are given in Figs. 7d and S7d, respectively. Based on calculated R^2 values, it can be concluded that the Langmuir isotherm, which is usually used to model the monolayer coverage, described the experimental data better than the Freundlich one. Alg polymer chains as well as MMT/Lap clays have a finite number of sorption sites, which favours monolayer formation [116].

Based on the maximum sorption capacity determined using the Langmuir model, it can be concluded that both C_{CaCl2} and clay content affect the sorption properties of the solids (Table S6). The largest q_m value was obtained for unfilled Alg synthesized using the smallest C_{CaCl2} equal to 0.25 wt%. The sorption of selected metal ions on the components of HGs occurred mainly through ion exchange with carboxyl groups [107,115]. An increase in the cross-linking degree reduced maximum sorption capacity of both unfilled and filled HGs, which was connected with the occupation of more carboxyl groups by Ca^{2+} ions. For example, for Alg, prepared using C_{CaCl2} of 0.25, 0.3, and 0.5 wt%, sorption capacity was 1.45, 1.36, and 1.26 mmol/g, respectively. Other researchers also noted that the presence of calcium and sodium salts reduced the sorption of heavy metals on Alg sorbents [131]. Nevertheless, the possibility of ion exchange between Ca^{2+} ions and Cd^{2+} ions during the sorption process cannot be excluded [107]. Cd^{2+} ion has better ion exchange properties due to stronger affinity for the biopolymers compared to Ca^{2+} one [131].

The dependences of maximum sorption capacity of Cd^{2+} ions on the Alg content in Alg/MMT and Alg/Lap are presented in Figs. 7e and S7e. At first it should be noted that so far, there have not been enough papers that describe the effect of clay filler and polymer contents in Alg-based composite HGs on heavy metal sorption [67]. In our case, increasing Alg content led to almost linear increase in sorption capacity of HGs. For composite HGs, the maximum q_m value was noted for the clay content of 20 wt%, for the samples synthesized with the minimum C_{CaCl2} of 0.25 wt %. This amounted to 1.24 and 1.38 mmol/g for Alg/20%MMT and Alg/20%Lap, respectively. Reducing Alg content to 50 wt% reduced sorption capacity to 0.84 and 1.26 mmol/g for Alg/50%MMT and Alg/50%Lap, respectively. It should be noted that the maximum sorption capacity of MMT and Lap were 0.063 and 0.639 mmol/g. The revealed sorption capacities of composite HGs, at neutral pH, turned out to be practically proportional to the sorption capacities of the components. The interactions between the components of the system (Alg and MMT, Alg and Lap) do not lead to a decrease in the sorption of metal ions.

Sorption capacity of Alg/Lap HGs towards Cd^{2+} ions was found to be greater than that of Alg/MMT HGs, which was associated with better sorption capacity of Lap (Table S6). A similar phenomenon was noted in [133]. At the same time, it was observed that the sorption of palladium (II) by Alg beads filled with MMT and Lap, prepared using 0.1 mol/L $CaCl_2$, was enhanced with increment of extracted/removed Pd(II) ion at pH 3 and 4 as well as in the presence of chloride ions. The revealed difference can be due to the fact that in our study we used Alg gels, the synthesis of which was optimized for the sorption of selected heavy metal ions. What is more, sorption isotherms were determined at significantly higher initial concentrations (up to 1000 mg/L), which allowed us to estimate the maximum sorption capacity more accurately. Nevertheless, for polysaccharide matrix with relatively low sorption properties, the contribution of fillers to the sorption capacity of the composite HGs can be decisive [134]. In exceptional cases, the maximum sorption of Cd(II) on alginate-based HGs with nanoclays can be lower than that on alginate-based HG without filler synthesized at the same concentration of cross-linking agent. This decrease was observed for Alg/MMT and was dictated by the sorption capacity of the applied filler - montmorillonite, which is lower than that of alginate. However, such a reduction was very insignificant, and the introduction of filler provided other structural and functional advantages when creating such composites.

To investigate mechanism of interactions of Cd^{2+} ions with composite HGs, the study on swelling degree of HGs after the Cd^{2+} sorption was performed. The HG sediment with sorbed Cd^{2+} ions was weighed and Q_∞ was determined using Eq. (2). The obtained data showed a rapid and significant reduction in swelling degree of both unfilled and filled HGs (Fig. S8). This allows to assume that Cd^{2+} cations can fill the space between the blocks of Alg polymers by a mechanism similar to the formation of network structure upon interactions with Ca^{2+} ions [74,135]. The decrease in Q_∞ for Alg/Lap was less pronounced than for Alg/MMT (Fig. S8). The swelling of Alg/Lap, when it was subjected to long-term exposure to 50 mg/L Cd^{2+} ions solutions, did not differ from that of unfilled Alg. The observed phenomenon can be explained by the greater sorption capacity of Lap compared to MMT. As a consequence, its contribution to the sorption of the heavy metal can be more significant, especially at low concentrations of Cd^{2+} ions.

3.3.4. Effect of pH

The pH value can affect significantly charge of functional groups in the polymer matrix, the metal form and solubility, and presence of charge-forming groups on nanoclay. In this way, it affects sorption capacity of composite HGs. Fig. 8a shows the variation of the Cd^{2+} ions removal efficiency as a function of pH value, whereas Fig. 8b presents the HG swelling degree after Cd^{2+} ions sorption at different pHs.

For initial Cd^{2+} ions concentration of 200 mg/L, the highest sorption in the pH range of 4–6 was found for unfilled Alg. The Cd^{2+} ions removal efficiency remained stable for unfilled Alg even with an increase in pH to 8–9 and amounted to 82 %. However, the sorption capacity of Alg was clearly reduced as pH decreased from pH 4 to pH 2. The swelling degree of unfilled Alg was also stable in the pH range of 4–9 and showed a decreasing trend when pH was reduced to 2. The observed phenomenon was related to the fact that the carboxyl groups of Alg were in the protonated form at pH below pK_a for mannuronic and guluronic acids and tendency to ionize at pH above 4 [118]. Thus, in the pH range of 4–7, sorption occurred mostly by the mechanism of electrostatic interactions, which gradually weaken with the decreasing pH [119]. Other authors noted a similar dependence of Cd^{2+} ions sorption on Alg in the pH range of 2–9 [118]. In most studies, heavy metal sorption studies were limited to neutral pH values, after which metal ions precipitation as hydroxides could occur [121,135]. However, in other studies, no evidence of Cd(II) hydroxide precipitation was found in blank experiments [117]. In our

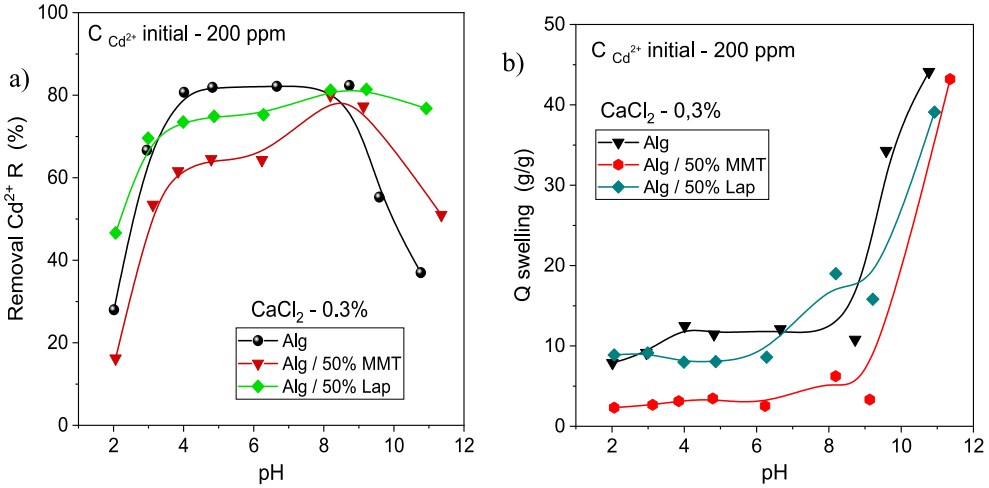

Fig. 8. Dependence of the removal efficiency of Cd^{2+} (a) and the swelling ratio of Alg, Alg/50%MMT, and Alg/50%Lap, prepared using 0.3 wt% of $CaCl_2$, after Cd^{2+} sorption at various pH values (b).

research, increasing the pH to 11 led to sharp drop in the Cd^{2+} ions sorption on Alg, which was simultaneously accompanied by significant increase in its swelling degree.

For Alg/MMT and Alg/Lap, stable levels of Cd^{2+} ions sorption were revealed in the pH range of 4–7, and they were slightly smaller than for those for unfilled Alg. Reducing pH to 2 decreased the ability of Alg/50%MMT and Alg/50%Lap to sorb Cd^{2+} ions to 16 and 47 %, respectively (for unfilled Alg, it was 28 %). Moreover, for Alg and Alg/50% MMT, a similar trend was noticed. It is known that Cd^{2+} ion is mainly sorbed on MMT by cation exchange [124], but hydroxyl groups (silanol, aluminum) located at the edges of clay can also be important [117]. Acidic conditions do not promote Cd^{2+} sorption since H_3O^+ ions compete with Cd^{2+} ions for active sites then [121,122]. Thus, at low pH values, the MMT impact on sorption capacity of the composite HGs is negative. Alg/50%Lap exhibited a significantly lower decline in sorption with the decreasing pH. On this solid, non-ionic mechanism of metal ion binding can occur, due to formation of hydrogen bonds with Lap hydroxyl groups.

Increasing the solution pH to 8–9 resulted in noticeable higher sorption of Cd, which can be associated with precipitation of metal hydroxide or augmentation of sorption on nanoclay plates. At pH above the point of zero charge (pH_{pzc}) for MMT (7.8) and for Lap (11.0), the clay surface generates negative charges through deprotonation, which promotes Cd^{2+} ions sorption [116,122,136]. The observed Cd^{2+} ions removal reached 80 and 81 % for Alg/50%MMT and Alg/50%Lap, respectively. Further increase in pH to 11 decreased insignificantly sorption capacity of Alg/50%Lap and Alg/50%MMT. However, the Cd^{2+} ions removal was higher for HGs with nanoclays than for unfilled Alg. At the same time, the increase in swelling degree increased significantly for both composite HGs and was comparable to Alg (Fig. 8b).

3.4. Cation exchange capacity and variable surface charge

Variable surface charge generated by negative functional groups of Lap, MMT, and Alg-based HGs are given in Fig. 9a, whereas relative fractions of $f(pK_{app})$ groups as a function of distribution of apparent surface dissociation constants are presented in Fig. 9b.

Among tested solids, Alg contained the highest amount of strongly acidic groups, and thus it was characterized by the highest variable surface charge. CEC (at pH 7) for unfilled Alg was 0.862 mmol/g, for Lap, 0.302 mmol/g, and for MMT, 0.326 mmol/g. The obtained CEC values for clay fillers were slightly smaller than those provided by other researchers [137,138]. This can be justified as the studies were carried out in 1 M NaCl, which can affect the net charge of solids besides pH

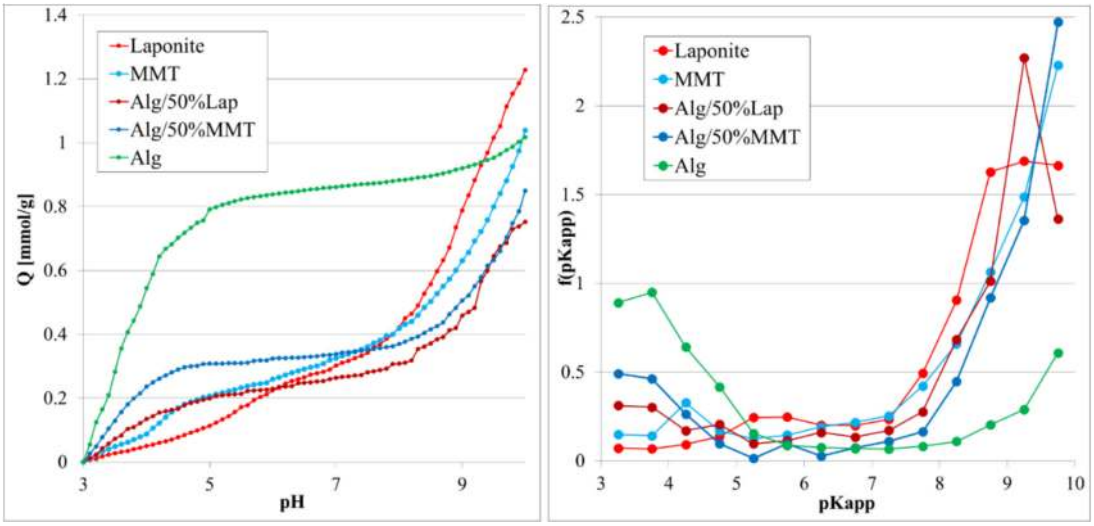

Fig. 9. Distribution of surface charge calculated from the titration curves (a) and surface dissociation constant distribution for Lap, MMT, Alg, Alg/50%Lap, and Alg/50%MMT (b). HGs were prepared using 0.3 wt% of $CaCl_2$.

[86]. Lap particles cannot generate a substantial pH-dependent surface charge in NaCl electrolyte due to the screening of electrostatic repulsive interactions between the negative charges on the clay surface [136]. This can also explain the overall decrease in CEC for composite HGs, compared to unfilled Alg, which were 0.264 and 0.338 mmol/g for Alg/50%Lap and Alg/50%MMT, respectively.

The potentiometric titration results showed that Lap presented the largest variable surface charge (Q_{var}) calculated at pH 10 compared to the other materials – 1.23 mmol/g. MMT and Alg were characterized by similar Q_{var} values, that is, 1.04 mmol/g (MMT) and 1.02 mmol/g, respectively. The variable surface charge of composite HGs decreased with the addition of Lap and MMT. At pH 10, the Q_{var} values were 0.751 mmol/g for Alg/50%Lap HG and 0.848 mmol/g for Alg/50%MMT. Since the method used is non-equilibrium and depends on empirically selected variables such as titration rate, solid-liquid ratios, etc., the obtained titration curves should be used rather for comparative studies [82]. Nevertheless, the trends in the CEC change with pH, obtained by potentiometric titration, correlated interestingly with the data for heavy metal sorption and those for HGs swelling depending on pH.

Thus, the Cd^{2+} sorption on alginate primarily occurs through ion exchange and chelation with carboxyl groups, with efficiency strongly dependent on pH and cross-linking density. In contrast, sorption on MMT and Lap involves ion exchange in the interlayer spaces, electrostatic attraction to negatively charged sites, and coordination to surface hydroxyl groups. The sorption mechanism of Cd^{2+} ions onto hybrid HGs filled with MMT and Lap involves a combination of ion exchange, surface complexation, and electrostatic interactions, modulated by the chemical properties of both Alg matrix and incorporated clay minerals. Alginate itself exhibited the highest CEC and a strong variable surface charge due to the abundance of carboxylic groups, enabling efficient binding of Cd^{2+} ions. However, the incorporation of Lap and MMT into the HG matrix led to a reduction in both CEC and variable surface charge (Q_{var}), as evidenced by potentiometric titration data. This suggests that the presence of clay fillers, while contributing structural and mechanical reinforcement, partially suppresses the ion-exchange and surface binding activity of the matrix. Despite this, the overall sorption mechanism on the composite hydrogels reflects the combined effects of Alg functional groups and clay layered structures, enabling effective Cd^{2+} immobilization through surface complexation and limited ion exchange.

3.5. Biosafety of HGs: Cytoto- and genotoxicity

To determine biosafety of HGs, the cytotoxicity and genotoxicity tests were performed. They are commonly used to select non-toxic and biocompatible materials [90].

Table 1 and Fig. 10 summarize the results of cytotoxicity test for intact cell control, DPBS control, and composite HGs prepared using C_{CaCl2} of 0.3 wt%. It was observed that the cell incubation without HGs reduced their metabolic activity (up to 82 %) and total number of adherent cells.

Table 1
Viability (% of live cells) of L-929 eukaryotic cells observed in the tests of HGs cytotoxicity with MTT and crystal violet.

Sample	x MTT, %	xx CV, %	Control DPBS		Cell control	
			x MTT, %	xx CV, %	x MTT, %	xx CV, %
Alg	98	100	82	82	97	97
Alg/20% Lap	88	100	82	82	97	97
Alg/50% Lap	81	93	82	82	97	97
Alg/20% MMT	75	90	82	82	97	97
Alg/50% MMT	92	97	82	82	97	97

Note: x MTT – the number of live cells in the MTT test, xx CV – the number of live cells in CV tests. Used in this study Alg-based hydrogels were synthesized using C_{CaCl2} of 0.3 wt%.

The medium conditioned with unfilled Alg did not give a cytotoxic effect. It statistically reduced the cytotoxic effect of DPBS both in terms of metabolic activity (by 16 %) and number of adherent cells (by 18 %). The media conditioned with Alg/20%Lap and Alg/50%Lap induced similar effect on metabolic activity of cells in all dilutions compared to the DPBS control. The percentage of adherent cells after the contact with Alg/50%Lap was almost 11 % greater, and Alg/20%Lap eliminated cytotoxic effect of DPBS completely. The reaction of cells to contact with Alg/MMT was not so clear. For the medium conditioned with Alg/20% MMT, metabolic activity of cells decreased slightly compared to the DPBS control, although in terms of percentage of adherent cells, the sample reduced statistically cytotoxic effect of DPBS by 8 %. In the case of medium conditioned with Alg/50%MMT, metabolic activity of cells at all dilutions did not decrease (compared to the DPBS control), and in terms of percentage of adherent cells, Alg/50%MMT also stimulated cell growth, reducing significantly cytotoxic effect of DPBS by 15 %. Thus, all the tested samples HGs at the tested concentration of 1 % did not exhibit cytotoxic effects on L-929 cells. Moreover, Alg, Alg/20%Lap, and Alg/50%MMT showed a growth-stimulating effect on eukaryotic cells.

The results of assessment of HGs genotoxicity relative to L-929 cells are presented in Table 2.

For all investigated HGs, there was no genotoxicity effect. All samples had I_{DNA} genotoxicity index at the level of negative control, which was represented by native cells, in contrast to the positive control – the cells treated with 1 mM nitrosourea.

4. Conclusions

The authors have developed new biocompatible, multifunctional materials that in the future can be used as soil conditioners, comprehensively improving its properties. A series of Alg-based composite hydrogels with varying concentrations of the cross-linking agent ($CaCl_2$) as well as MMT or LaponiteRD nanoclay fillers were synthesized and characterized in detail. The main attention was paid to the study of composite HGs swelling and sorption abilities towards heavy metal ions – Cd^{2+}. The paper presents a number of innovative aspects in the field of polymer-clay composites for heavy metal sorption and environmental applications. For example, the influence of the concentration and type of mineral fillers, the degree of cross-linking, as well as environmental factors (in particular, pH) on the sorption capacity of materials for Cd^{2+} ions were systematically investigated. The patterns of changes in the swelling mechanism of hydrogels (from Fickian to non-Fickian) with increasing cross-linker concentration indicated the correlation between the structural parameters of composites and their sorption efficiency, as well as confirmed the chemical mechanism of sorption without desorption.

SEM indicated homogeneous distribution of MMT and Lap particles with the formation of layered structure, whereas FTIR confirmed interactions between nanoclay and polymer carboxyl groups. The synthesized composite HGs showed high swelling degrees up to 100 g/g as well as great sorption capacity for Cd^{2+} ions up to 1.2 mmol/g. Their equilibrium swelling degree decreased with an increase in the cross-linker concentration as well as in the content of nanoclay filler. It was found that for Alg and Alg/Lap, the optimal C_{CaCl2} was 0.3 wt%, whilst for Alg/MMT, 0.25 wt%. At this C_{CaCl2}, stable composite HGs with high swelling degree (up to 50–70 g/g), of strength sufficient for environmental purification, were obtained. The synthesized composite HGs showed great sorption capacity for Cd^{2+} ions. At low C_{eq}, the highest efficiency in the Cd^{2+} ions removal was observed for Alg/Lap (up to 97.8 %) due to numerous active sites of the applied clay.

The developed effects of the filler content and the cross-linking agent concentration on the HGs swelling and sorption towards Cd^{2+} ions, as well as and the investigated mechanisms of these processes allowed for

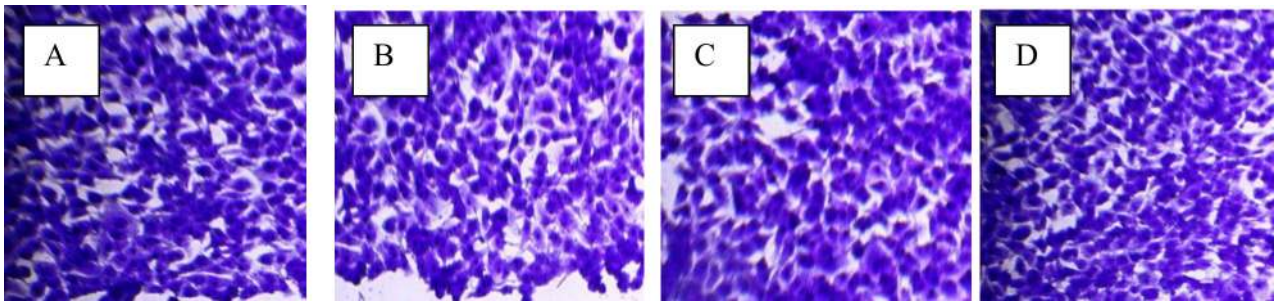

Fig. 10. Image of L-929 cell culture in the field of view of light microscope, stained with crystal violet (magnification 400x): A – L-929 cells in DMEM/F12 (cell control), B – L-929 cells in DMEM/F12 with DPBS (control DPBS), C – L-929 cells grown for 24 h in DMEM/F12 with Alg/50%Lap in DPBS, D – L-929 cells grown for 24 h in DMEM/F12 with Alg in DPBS (all cells were grown for 24 h). (For interpretation of the references to colour in this figure legend, the reader is referred to the web version of this article.)

Table 2
The results of in vitro studies of HGs genotoxicity.

Sample	I_{DNA}	Conclusion
Negative control (untreated cells L929)	0.49 ± 0.01	not genotoxic
Positive control (cells treated with mutagen −1 mM nitrosourea)	1.24 ± 0.02	genotoxic
Alg	0.55 ± 0.01	not genotoxic
Alg/20%Lap	0.49 ± 0.01	not genotoxic
Alg/50%Lap	0.48 ± 0.02	not genotoxic
Alg/20%MMT	0.50 ± 0.01	not genotoxic
Alg/50%MMT	0.52 ± 0.02	not genotoxic

effective regulation of synthesis conditions and optimization of HGs composition. The investigated dependencies opened up opportunities of composite HGs application as soil conditioners, which are capable of significant improving water-holding properties of the soils as well as of cadmium immobilization preventing its entry into crops. The absence of cyto- and genotoxicity confirmed the biological safety of the prepared materials, which allowed their long-term use in the environment.

Abbreviations

Alg	Alginate
Na-Alg	sodium alginate
HG	Hydrogel
MMT	Montmorillonite
Lap	LaponiteRD
SEM	Scanning Electron Microscopy
EDX	Energy Dispersive X-ray Spectroscopy
FTIR	Fourier-Transform Infrared Spectroscopy
XRD	X-ray Diffraction
CEC	Cation exchange capacity
DPBS	Dulbecco's phosphate-buffered saline
DNA	deoxyribonucleic acid
MTT	thiazolyl blue tetrazolium bromide
L-929	mouse fibroblast cell culture
EDTA	Ethylenediaminetetraacetic acid
DMSO	Dimethyl sulfoxide
DMEM/F12	Dulbecco's Modified Eagle Medium/Nutrient Mixture F-12
ATCC	American Type Culture Collection
CCL-1™	name of clone L929 from the ATCC collection
C_{CaCl2}	$CaCl_2$ concentration

CRediT authorship contribution statement

Nataliia Guzenko: Writing – original draft, Visualization, Validation, Methodology, Investigation, Data curation. **Olena Goncharuk:** Writing – review & editing, Validation, Supervision, Project administration, Conceptualization. **Yurii Samchenko:** Investigation, Conceptualization. **Konrad Terpiłowski:** Investigation. **Katarzyna Grygorczuk-Płaneta:** Investigation, Data curation. **Svitlana Dybkova:** Writing – original draft, Investigation. **Bartosz Kondracki:** Investigation. **Katarzyna Szewczuk-Karpisz:** Writing – review & editing, Supervision.

Funding sources

Polish Academy of Sciences and the U.S. National Academy of Sciences financial support. Agreement No. PAN.BFB.S.BWZ.331.022.2023 «Biocompatible hybrid hydrogels with functional inorganic fillers for strengthening of plant vegetation».

Declaration of competing interest

The authors declare that they have no known competing financial interests or personal relationships that could have appeared to influence the work reported in this paper.

Acknowledgments

The authors, N. Guzenko, O. Goncharuk, Yu. Samchenko, and S. Dybkova, are grateful for the financial support of the Polish Academy of Sciences and the U.S. National Academy of Sciences (Agreement No. PAN.BFB.S.BWZ.331.022.2023 «Biocompatible hybrid hydrogels with functional inorganic fillers for strengthening of plant vegetation»). O. Goncharuk thanks to the European Chemistry School for supporting Ukrainian scientists in 2025.

Appendix A. Supplementary data

Supplementary data to this article can be found online at https://doi.org/10.1016/j.ijbiomac.2025.145870.

References

[1] K. Rehman Hakeem, M. Öztürk, M. Sabir, A.R. Mermut, Soil remediation and plants: prospects and challenges, Academic Press, 2015, https://doi.org/10.1016/C2013-0-13078-4.
[2] Nordberg, G.F., Fowler, B.A., Nordberg, M. Handbook on the Toxicology of Metals (4th ed.), Academic Press, 2015. https://doi.org/10.1016/B978-0-444-59453-2.05001-0.
[3] World Health Organization. Guidelines for drinking-water quality, 4th edition incorporating the 1st addendum. WHO Press, Geneva, 2017. 978–92–4–154995–0. https://www.who.int/publications/i/item/9789241549950.
[4] C. Doccioli, F. Sera, A. Francavilla, A. Cupisti, A. Biggeri, Association of cadmium environmental exposure with chronic kidney disease: a systematic review and meta-analysis, Sci. Total Environ. 906 (2024) 167165, https://doi.org/10.1016/j.scitotenv.2023.167165.

[5] Y. Ma, D. Ran, X. Shi, H. Zhoao, Z. Liu, Cadmium toxicity: a role in bone cell function and teeth development, Sci. Total Environ. 734 (2021) 139419, https://doi.org/10.1016/j.scitotenv.2020.139419.
[6] Huff, J.; Lunn, R.M.; Waalkes, M.P.; Tomatis, L.; Infante, P.F. Cadmium-induced cancers in animals and in humans. Int. J. Occup. Environ. Health, 16(2), 96-101. https://doi.org/10.1179/oeh.2009.16.2.96.
[7] L. Järup, Hazards of heavy metal contamination, Br. Med. Bull. 68 (1) (2003) 167–182, https://doi.org/10.1093/bmb/ldg032.
[8] K. Zaman, A. Elahi, D.A. Bukhari, A. Rehman, Cadmium sources, toxicity, resistance and removal by microorganisms – a potential strategy for cadmium eradication, J. Saudi Chem. Soc. 26 (6) (2022) 101569, https://doi.org/10.1016/j.jscs.2022.101569.
[9] F.J. Zhao, Y. Ma, Y.G. Zhu, Z. Tang, Soil contamination in China: current status and mitigation strategies, Environ. Sci. Technol. 49 (2) (2015) 750–759, https://doi.org/10.1021/es5047099.
[10] C.A. Grant, W.T. Buckley, L.D. Bailey, F. Selles, Cadmium accumulation in crops, Can. J. Plant Sci. 78 (1) (1998) 1–17, https://doi.org/10.4141/P96-100.
[11] Z.L. He, X.E. Yang, P.J. Stoffella, Trace elements in agroecosystems and impacts on the environment, J. Trace Elem. Med. Biol. 19 (2–3) (2005) 125–140, https://doi.org/10.1016/j.jtemb.2005.02.010.
[12] M. Sun, T. Wang, X. Xu, L. Zhang, J. Li, Y. Shi, Ecological risk assessment of soil cadmium in China's coastal economic development zone: a meta-analysis, Ecosyst. Health Sustain. 6 (1) (2020) 1733921, https://doi.org/10.1080/20964129.2020.1733921.
[13] W. Xu, L. Xiao, S. Hou, Bioavailability and speciation of cadmium in contaminated paddy soil as alleviated by biochar from co-pyrolysis of peanut shells and maize straw, Environ. Sci. Eur. 34 (2022) 69, https://doi.org/10.1186/s12302-022-00650-y.
[14] X. Huang, X. Li, L. Zheng, Y. Zhang, L. Sun, Y. Feng, J. Du, X. Lu, G. Wang, Comprehensive assessment of health and ecological risk of cadmium in agricultural soils across China: a tiered framework, J. Hazard. Mater. 465 (2024) 133111, https://doi.org/10.1016/j.jhazmat.2023.133111.
[15] X. Tian, G. Chai, Q. Xie, Risk identification of heavy metals in agricultural soils from a typically high Cd geological background area in upper reaches of the Yangtze River, Bull. Environ. Contam. Toxicol. 109 (2022) 713–718, https://doi.org/10.1007/s00128-021-03417-y.
[16] M. Zakrzewska, G. Rzepa, M. Musialowski, A. Goszcz, R. Stasiuk, K. Debiec-Andrzejewska, Reduction of bioavailability and phytotoxicity effect of cadmium in soil by microbial-induced carbonate precipitation using metabolites of ureolytic bacterium *Ochrobactrum* sp. POC9, Front. Plant Sci. 14 (2023) 1–18, https://doi.org/10.3389/fpls.2023.1109467.
[17] M. Rahimi, G. Rahimi, E. Ebrahimi, Assessing the distribution of cadmium under different land-use types and its effect on human health in different gender and age groups, Environ. Sci. Pollut. Res. 28 (2021) 49258–49267, https://doi.org/10.1007/s11356-021-12881-2.
[18] Sh.Al. Mamun, Sh. Saha, J. Ferdush, T.R. Tusher, M. Abu-Sharif, M.F. Alam, M. R. Balks, Z. Parveen, Cadmium contamination in agricultural soils of Bangladesh and management by application of organic amendments: evaluation of field assessment and pot experiments, Environ. Geochem. Health 43 (9) (2021) 3557–3582, https://doi.org/10.1007/s10653-021-00829-x.
[19] K. Kameyama, T. Miyamoto, Y. Iwata, Comparison of plant cd accumulation from a cd-contaminated soil amended with biochar produced from various feedstocks, Environ. Sci. Pollut. Res. Int. 28 (10) (2021) 12699–12706, https://doi.org/10.1007/s11356-020-11249-2.
[20] T. Arao, S. Ishikawa, M. Murakami, K. Abe, Y. Maejima, T. Makino, Heavy metal contamination of agricultural soil and countermeasures in Japan, Paddy Water Environ. 8 (2010) 247–257, https://doi.org/10.1007/s10333-010-0205-7.
[21] C.A. Adarme-Duran, J. Ágreda, P.F.B. Brandão, Cadmium availability in rhizosphere and non-rhizosphere soils in cacao farms in Santander, Colombia, Environ. Monit. Assess. 196 (2024) 1254, https://doi.org/10.1007/s10661-024-13301-x.
[22] K. Carrillo, M. Martínez, L. Ramírez, D. Argüello, E. Chavez, Cadmium (cd) distribution and soil plant relationship in cacao farms in Costa Rica, Environ. Monit. Assess. 195 (10) (2023) 1209.
[23] Meter, A.; Atkinson, R. J.; Laliberte, B. Cadmium in cacao from Latin America and the Caribbean. A review of research and potential mitigation solutions. Bioversity International 2019, 73. Available online: https://hdl.handle.net/ 10568/102353.
[24] N.R. Maddela, D. Kakarla, L.C. García, S. Chakraborty, K. Venkateswarlu, M. Megharaj, Cacao-laden cadmium threatens human health and cacao economy: a critical view, Sci. Total Environ. 720 (2020) 137645, https://doi.org/10.1016/j.scitotenv.2020.137645.
[25] T. Sterckeman, L. Gossiaux, S. Guimont, C. Sirguey, Z. Lin, Cadmium mass balance in French soils under annual crops: scenarios for the next century, Sci. Total Environ. 639 (2018) 1440–1452, https://doi.org/10.1016/j.scitotenv.2018.05.225.
[26] J. Zhang, A. Hao, B. Zhao, F. Ma, X. Zhang, Y. Zhang, K. Duan, Y. Li, Effects of microplastics and cadmium co-contamination on soil properties, maize (Zea mays L.) growth characteristics, and cadmium accumulation in maize in loessial soil-maize systems, Environ. Pollut. 356 (2024) 124363, https://doi.org/10.1016/j.envpol.2024.124363.
[27] T. Sterckeman, M. Puschenreiter, Phytoextraction of cadmium: feasibility in field applications and potential use of harvested biomass, in: A. Van der Ent, G. Echevarria, A.J.M. Baker, J.L. Morel (Eds.), Agromining: farming for metals: extracting unconventional resources using plants, Springer International Publishing, Cham, 2018.
[28] Y. Deng, S. Fu, M. Xu, H. Liu, L. Jiang, X. Liu, H. Jiang, Purification and water resource circulation utilization of cd-containing wastewater during microbial remediation of cd-polluted soil, Environ. Res. 219 (2023) 115036, https://doi.org/10.1016/j.envres.2022.115036.
[29] S. Satyam, S. Patra, Innovations and challenges in adsorption-based wastewater remediation: a comprehensive review, Heliyon (2024) e29573, https://doi.org/10.1016/j.heliyon.2024.e29573.
[30] N.T. Pessôa, D.C.S. Sales, G.E. Nascimento, J.H.L. Santos, M.N. Santos Silva, D. C. Napoleão, J.M. Rodríguez-Díaz, M.M.M.B. Duarte, Effective adsorption of cadmium and nickel ions in mono and bicomponent systems using eco-friendly adsorbents prepared from peanut shells, Environ. Res. 247 (2024) 118220, https://doi.org/10.1016/j.envres.2024.118220.
[31] X. Pei, L. Gan, Z. Tong, H. Gao, S. Meng, W. Zhang, P. Wang, Y. Chen, Robust cellulose-based composite adsorption membrane for heavy metal removal, J. Hazard. Mater. 406 (2021) 124746, https://doi.org/10.1016/j.jhazmat.2020.124746.
[32] M. Vera, D.M. Juela, C. Cruzat, E. Vanegas, Modeling and computational fluid dynamic simulation of acetaminophen adsorption using sugarcane bagasse, J. Environ. Chem. Eng. 9 (2021) 105056, https://doi.org/10.1016/J.JECE.2021.105056.
[33] A.S. Morshedy, A.A. Galhoum, A.A.H.A. Aleem, M.T.Sh. El-din, D.M. Okaba, M. S. Mostafa, H.I. Mira, Z. Yang, I.E.T. El-Sayed, Functionalized aminophosphonate chitosan-magnetic nanocomposites for Cd(II) removal from aqueous solutions: performance and mechanisms of sorption, Appl. Surf. Sci. 561 (2021) 150069, https://doi.org/10.1016/j.apsusc.2021.150069.
[34] X. Qiu, B. Wang, X. Zhao, X. Zhou, R. Wang, Green and sustainable imprinting technology for removal of heavy metal ions from water via selective adsorption, Sustainability 16 (339) (2024), https://doi.org/10.3390/SU16010339.
[35] L.R. Rao, B.D. Dinesh, S. Mekala, J.R. Babu, K. Ravindhranath, Novel adsorbents for the removal of toxic cadmium ions from polluted water, Int. J. Phytoremediation 25 (9) (2023) 1127–1141, https://doi.org/10.1080/15226514.2022.2137101.
[36] B. Wang, B. Gao, Y. Wan, Entrapment of ball-milled biochar in ca-alginate beads for the removal of aqueous cd(II), J. Ind. Eng. Chem. 61 (2018) 161–168, https://doi.org/10.1016/j.jiec.2017.12.013.
[37] X. Mei, H. Yuan, L. He, Adsorption of Cd(II) by montmorillonite modified with biochar: mechanisms and potential application for water remediation, Water Res. 159 (2019) 411–420.
[38] X. Cao, B. Yan, Y. Huang, Y. Zhang, L. Li, J. Qiu, X. Lyu, Use of Laponite as adsorbents for Ni(II) removal from aqueous solution, Environ. Prog. Sustain. Energy 37 (3) (2017) 942–950, https://doi.org/10.1002/ep.12749.
[39] F. Ahmadi, H. Esmaeili, Chemically modified bentonite/Fe3O4 nanocomposite for Pb(II), Cd(II), and Ni(II) removal from synthetic wastewater, Desalin. Water Treat. 110 (2018) 154–167, https://doi.org/10.5004/dwt.2018.22228.
[40] V.L. Díaz de Rosa, A.V. Gil Rebaza, M.L. Montes, M.A. Taylor, R.E. Alonso, Sorption of Sr on montmorillonite clays: theoretical and experimental study, Appl. Surf. Sci. 592 (2022) 153146, https://doi.org/10.1016/j.apsusc.2022.153146.
[41] V.B. Yadav, R. Gadi, S. Kalra, Clay-based nanocomposites for removal of heavy metals from water: a review, J. Environ. Manag. 232 (2019) 803–817, https://doi.org/10.1016/j.jenvman.2018.11.120.
[42] A.S. Ozcan, A. Ozcan, Adsorption of acid dyes from aqueous solutions onto acid-activated bentonite, J. Colloid Interface Sci. 276 (2004) 39–46, https://doi.org/10.1016/j.jcis.2004.03.043.
[43] H. Alkhaldi, S. Alharthi, S. Alharthi, H.A. AlGhamdi, Y.M. AlZahrani, S. A. Mahmoud, L.G. Amin, N.H. Al-Shaalan, W.E. Boraie, M.S. Attia, S.A. Al-Gahtany, N. Aldaleeli, M.M. Ghobashy, A.I. Sharshir, M. Madani, R. Darwesh, S. F. Abaza, Sustainable polymeric adsorbents for adsorption-based water remediation and pathogen deactivation: a review, RSC Adv. 14 (2024) 33143–33190, https://doi.org/10.1039/D4RA05269B.
[44] Z. Darban, S. Shahabuddin, R. Gaur, I. Ahmad, N. Sridewi, Hydrogel-based adsorbent material for the effective removal of heavy metals from wastewater: a comprehensive review, Gels 8 (2022) 263, https://doi.org/10.3390/gels8050263.
[45] X. Qiu, B. Wang, X. Zhao, X. Zhou, R. Wang, Green and sustainable imprinting technology for removal of heavy metal ions from water via selective adsorption, Sustainability 16 (2023) 339, https://doi.org/10.3390/SU16010339.
[46] G. Zhou, J. Luo, C. Liu, L. Chu, J. Crittenden, Efficient heavy metal removal from industrial melting effluent using fixed-bed process based on porous hydrogel adsorbents, Water Res. 131 (2018) 246–254, https://doi.org/10.1016/j.watres.2017.12.067.
[47] C. Jiang, X. Wang, G. Wang, C. Hao, X. Li, T. Li, Adsorption performance of a polysaccharide composite hydrogel based on crosslinked glucan/chitosan for heavy metal ions, Compos. B Eng. 169 (2019) 45–54, https://doi.org/10.1016/j.compositesb.2019.03.082.
[48] B. Zhao, H. Jiang, Z. Lin, S. Xu, J. Xie, A. Zhang, Preparation of acrylamide/acrylic acid cellulose hydrogels for the adsorption of heavy metal ions, Carbohydr. Polym. 224 (2019) 115022, https://doi.org/10.1016/j.carbpol.2019.115022.
[49] X. Gao, C. Guo, J. Hao, Z. Zhao, H. Long, M. Li, Adsorption of heavy metal ions by sodium alginate based adsorbent – a review and new perspectives, Int. J. Biol. Macromol. 164 (2020) 4423–4434, https://doi.org/10.1016/j.ijbiomac.2020.09.046.
[50] K.Z. Elwakeel, M.M. Ahmeda, A. Akhdhara, M.G.M. Sulaimana, Z.A. Khan, Recent advances in alginate-based adsorbents for heavy metal retention from water: a

review, Desalin. Water Treat. 272 (2022) 50–74, https://doi.org/10.5004/dwt.2022.28834.
[51] W. Zhang, J. Ou, B. Wang, H. Wang, Q. He, J. Song, H. Zhang, M. Tang, L. Zhou, Y. Gao, S. Sun, Efficient heavy metal removal from water by alginate-based porous nanocomposite hydrogels: the enhanced removal mechanism and influencing factor insight, J. Hazard. Mater. 418 (2021) 126358, https://doi.org/10.1016/j.jhazmat.2021.126358.
[52] A. Kumar, A. Kothari, P. Kumar, A. Singh, K. Tripathi, J. Gairolla, M. Pai, B. J. Omar, Introduction to alginate: biocompatible, biodegradable, antimicrobial nature and various applications, Alginate - Applications and Future Perspectives, IntechOpen. (2023), https://doi.org/10.5772/intechopen.110650.
[53] A.K. Thakur, M. Kumar, Efficacy of green alginate beads for multi-metal removal from aqueous solution, Case Stud. Chem. Environ. Eng. 3 (2021) 100100, https://doi.org/10.1016/j.cscee.2021.100100.
[54] M. Esmat, A.A. Farghali, M.H. Khedr, I.M. El-Sherbiny, Alginate-based nanocomposites for efficient removal of heavy metal ions, Int. J. Biol. Macromol. 102 (2017) 272–283, https://doi.org/10.1016/j.ijbiomac.2017.04.021.
[55] L. Pan, Z. Wang, X. Zhao, H. He, Efficient removal of lead and copper ions from water by enhanced strength-toughness alginate composite fibers, Int. J. Biol. Macromol. 134 (2019) 223–229, https://doi.org/10.1016/j.ijbiomac.2019.05.022.
[56] B. Wang, Y. Wan, Y. Zheng, X. Lee, T. Liu, Z. Yu, J. Huang, Y.S. Ok, J. Chen, B. Gao, Alginate-based composites for environmental applications, Crit. Rev. Environ. Sci. Technol. 49 (4) (2018) 318–356, https://doi.org/10.1080/10643389.2018.1547621.
[57] A.A. Oladipo, M. Gazi, Enhanced removal of crystal violet by low cost alginate/acid activated bentonite composite beads: optimization and modelling using non-linear regression technique, J. Water Process Eng. 2 (2014) 43–52, https://doi.org/10.1016/j.jwpe.2014.04.007.
[58] X.-M. Zheng, J.-F. Dou, M. Xia, A.-Z. Ding, Ammonium-pillared montmorillonite-$CoFe_2O_4$ composite caged in calcium alginate beads for the removal of Cs^+ from wastewater, Carbohydr. Polym. 167 (2017) 306–316, https://doi.org/10.1016/j.carbpol.2017.03.059.
[59] M. Râpă, E. Matei, A. Ţurcanu, A.M. Predescu, M.C. Pantilimon, C. Predescu, Structural, morphological and thermal analysis of some alginate/starch/dellite HPS composites for aqueous cu(II) removal, Cellul. Chem. Technol. 53 (2019) 5–6, https://doi.org/10.35812/CelluloseChemTechnol.2019.53.56.
[60] F. Alcalde-Garcia, S. Prasher, S. Kaliaguine, J.R. Tavares, M.-J. Dumont, Desorption strategies and reusability of biopolymeric adsorbents and semisynthetic derivatives in hydrogel and hydrogel composites used in adsorption processes, ACS Eng. Au. 3 (2023) 443–460, https://doi.org/10.1021/acsengineeringau.3c00022.
[61] G.B. Marandi, M. Baharloui, M. Kurdtabar, L.M. Sharabian, M. Mojarrad, Hydrogel with high laponite content as nanoclay: swelling and cationic dye adsorption properties, Res. Chem. Intermed. 41 (2015) 7043–7058, https://doi.org/10.1007/s11164-014-1797-0.
[62] E. Munoz-Perez, A. Perez-Valle, M. Igartua, E. Santos-Vizcaino, R.M. Hernandez, High resolution and fidelity 3D printing of Laponite and alginate ink hydrogels for tunable biomedical applications, Biomater. Adv. 149 (2023) 213414, https://doi.org/10.1016/j.bioadv.2023.213414.
[63] R.R. Pawar, Lalhmunsiama, P.G. Ingole, S.-M. Lee, Use of activated bentonite-alginate composite beads for efficient removal of toxic Cu^{2+} and Pb^{2+} ions from aquatic environment, Int. J. Biol. Macromol. 164 (2020) 3145–3154, https://doi.org/10.1016/j.ijbiomac.2020.08.130.
[64] K. Attar, H. Demey, D. Bouazza, A.M. Sastre, Sorption and desorption studies of Pb(II) and Ni(II) from aqueous solutions by a new composite based on alginate and magadiite materials, Polymers (Basel). 11 (2) (2019) 340, https://doi.org/10.3390/polym11020340.
[65] R. Aziam, D.S. Stefan, S. Nouaa, M. Chiban, M. Boşomoiu, Adsorption of metal ions from single and binary aqueous systems on bio-nanocomposite, alginate-clay, Nanomaterials 14 (4) (2024) 362, https://doi.org/10.3390/nano14040362.
[66] M. Râpă, A.A. Ţurcanu, E. Matei, A.M. Predescu, M.C. Pantilimon, G. Coman, C. Predescu, Adsorption of copper (II) from aqueous solutions with alginate/clay hybrid materials, Materials 14 (23) (2021) 7187, https://doi.org/10.3390/ma14237187.
[67] H.A. Shawky, Improvement of water quality using alginate/montmorillonite composite beads, J. Appl. Polym. Sci. 119 (4) (2011) 2371–2378, https://doi.org/10.1002/app.32694.
[68] I. Pylypenko, I. Kovalchuk, M. Tsyba, Development of granular composites based on laponite and Zr/Fe-alginate for effective removal of uranium (VI) from sulfate solutions, Eastern-European Journal of Enterprise Technologies 6 (2023) 27–34, https://doi.org/10.15587/1729-4061.2023.292524.
[69] A. Mourpichai, T. Jintakosol, W. Nitayaphat, Adsorption of gold ion from a solution using montmorillonite/alginate composite, Mater. Today Proc. 5 (2018) 7, https://doi.org/10.1016/j.matpr.2018.04.006.
[70] R. Foroutan, A. Mogammadzadeh, S. Javanbakht, R. Mohammadi, M. Ghorbani, Alginate/magnetic hydroxyapatite bio-nanocomposite hydrogel bead as a pH-responsive oral drug carrier for potential colon cancer therapy, Res. Chem. 12 (2025) 102177, https://doi.org/10.1016/j.rechem.2025.102177.
[71] R. Foroutan, S.J. Peighambardoust, S. Ghojavand, S. Farjadfard, B. Ramavandi, Cadmium elimination from wastewater using potato peel biochar modified by ZIF-8 and magnetic nanoparticle, Colloid. Interface Sci. Commun. 55 (2023) 100723, https://doi.org/10.1016/j.colcom.2023.100723.
[72] B. Naeimi, R. Foroutan, B. Ahmadi, F. Sadeghzadeh, B. Ramavandi, Pb(II) and cd (II) removal from aqueous solution, shipyard wastewater, and landfill leachate by modified Rhizopus oryzae biomass, Mater. Res. Express 5 (2018) 045501, https://doi.org/10.1088/2053-1591/aab81b.
[73] M. Alizadeh, S.J. Peighambardoust, R. Foroutan, Efficious adsorption of divalent nickel ions over sodium alginate-g-poly(acrylamide)/hydrolyzed *Luffa* cylindrical-CoFe2O4 bionanocomposite hydrogel, Int. J. Biol. Macromol. 254 (1) (2024) 127750, https://doi.org/10.1016/j.ijbiomac.2023.127750.
[74] H. Malektaj, A.D. Drozdov, J. de Claville Christiansen, Mechanical properties of alginate hydrogels cross-linked with multivalent cations, Polymers (Basel) 15 (2023) 3012, https://doi.org/10.3390/polym15143012.
[75] S. Cetaldo, N. Muratore, S. Oreccio, A. Pettignano, Enhancement of adsorption ability of calcium alginate gel beads towards Pd(II) ion. A kinetic and equilibrium study on hybrid Laponite and montmorillonite-alginate gel beads, Appl. Clay Sci. 118 (2015) 162–170, https://doi.org/10.1016/j.clay.2015.09.014.
[76] L.C. Bandeira, P.S. Calefi, K.J. Ciuffi, E.H. de Faria, E.J. Nassar, M.A. Vicente, R. Trujillano, Preparation of composites of laponite with alginate and alginic acid polysaccharides, Polym. Int. 61 (2012) 7, https://doi.org/10.1002/pi.4196.
[77] V. Gopalakannan, S. Periyasamy, N. Viswanathan, Synthesis of assorted metal ions anchored alginate bentonite biocomposites for Cr(VI) sorption, Carbohydr. Polym. 151 (2016) 1100–1109, https://doi.org/10.1016/j.carbpol.2016.06.030.
[78] A. Ely, M. Baudu, J.-P. Basly, M.O.S.A. Kankou, Copper and nitrophenol pollutants removal by Na-montmorillonite/alginate microcapsules, J. Hazard. Mater. 171 (2009) 405–409, https://doi.org/10.1016/j.jhazmat.2009.06.015.
[79] O. Goncharuk, O. Siryk, M. Frąc, N. Guzenko, K. Samchenko, K. Terpiłowski, D. Sternik, K. Szewczuk-Karpisz, Synthesis, characterization and biocompatibility of hybrid hydrogels based on alginate, κ-carrageenan, and chitosan filled with montmorillonite clay, Int. J. Biol. Macromol. 278 (2) (2024) 134703, https://doi.org/10.1016/j.ijbiomac.2024.134703.
[80] O. Siryk, O. Goncharuk, Y. Samchenko, L. Kernosenko, K. Szewczuk-Karpisz, Comparison of structural, water-retaining and sorption properties of acrylamide-based hydrogels cross-linked by physical and chemical methods, ChemPhysChem 25 (4) (2023) e202300812, https://doi.org/10.1002/cphc.202300812.
[81] H. Malektaj, A.D. Drozdov, J. de Claville Christiansen, Swelling of homogeneous alginate gels with multi-stimuli sensitivity, Int. J. Mol. Sci. 24 (2023) 5064, https://doi.org/10.3390/ijms24065064.
[82] J. Joseph, M. Webber, G. Worste, A linear-elastic-nonlinear-swelling theory for hydrogels. Part 1. Modelling of super-absorbent gels, J. Fluid Mech. 960 (2023) A37, https://doi.org/10.1017/jfm.2023.200.
[83] G. Józefaciuk, J.S. Shin, Water vapor adsorption on soils: II. Estimation of adsorption energy distributions using local BET and Aranovich isotherms, Korean J. Soil Sci. Fert. 29 (3) (1996) 218–225.
[84] D. Matyka-Sarzyńska, Z. Sokołowska, Physicochemical properties of mucks at different stage of secondary transformations (in polish), Acta Agrophysica 123 (2005) 1–68.
[85] K. Skic, P. Boguta, Z. Sokołowska, Analysis of the sorption properties of different soils using water vapour adsorption and potentiometric titration methods, Int. Agrophys. 30 (2016) 369–374, https://doi.org/10.1515/intag-2015-0100.
[86] G. Kiaee, N. Dimitrakakis, S. Sharifzadeh, H.J. Kim, R.K. Avery, K. M. Moghaddam, R. Haghniaz, E.P. Yalcintas, N.R. Barros, S. Karamikamkar, A. Libanori, A. Khademhosseini, P. Khoshakhlagh, Laponite-based nanomaterials for drug delivery, Adv. Healthc. Mater. 11 (7) (2022) e2102054, https://doi.org/10.1002/adhm.202102054.
[87] E.D. Revellame, D.L. Fortela, W. Sharp, R. Hernandez, M.E. Zappi, Adsorption kinetic modeling using pseudo-first order and pseudo-second order rate laws: a review, Clean. Eng. Technol. 1 (2020) 100032, https://doi.org/10.1016/j.clet.2020.100032.
[88] Y. Ho, G. McKay, Pseudo-second order model for sorption processes, Process Biochem. 34 (5) (1999) 451–465, https://doi.org/10.1016/S0032-9592(98)00112-5.
[89] Y.S. Ho, G. McKay, Sorption of dye from aqueous solution by peat, Chem. Eng. J. 70 (1998) 115–124.
[90] ISO 10993–5:2009. Biological evaluation of medical devices - part 5: test for in vitro cytotoxicity. The standard was last reviewed and confirmed in 2022.
[91] L. Śliwka, K. Wiktorska, P. Suchocki, M. Milczarek, Sz Mielczarek, K. Lubelska, T. Cierpiał, P. Łyżwa, P. Kiełbasiński, A. Jaromin, A. Flis, Z. Chilmonczyk, The comparison of MTT and CVS assays for the assessment of anticancer agent interactions, PLoS One 11 (5) (2016) e0155772, https://doi.org/10.1371/journal.pone.0155772.
[92] K. Chiba, K. Kawakami, K. Tohyama, Simultaneous evaluation of cell viability by neutral red, MTT and crystal violet staining assays of the same cells, Toxicol. in Vitro 12 (3) (1998) 251–258, https://doi.org/10.1016/S0887-2333(97)00107-0.
[93] P.L. Olive, The comet assay: an overview of techniques, Methods Mol. Biol. 203 (2002) 179–194, https://doi.org/10.1385/1-59259-179-5:179.
[94] A.R. Collins, The comet assay for DNA damage and repair: principles, applications and limitations, Mol. Biotechnol. 26 (3) (2004) 249–261, https://doi.org/10.1385/MB:26:3:249.
[95] Didenko, V.V. In situ detection of DNA damage. Methods Mol. Biol. 2002, 203, 299. https://doi.org/10.1385/1592591795.
[96] L. Bippus, M. Jaber, B. Lebeau, Laponite and hybrid surfactant/laponite particles processed as spheres by spray-drying, New J. Chem. 33 (2009) 1116–1126, https://doi.org/10.1039/b820429b.
[97] C. Yu, X. Tang, S. Liu, Y. Yang, X. Shen, C. Gao, Laponite crosslinked starch/polyvinyl alcohol hydrogels by freezing/thawing process and studying their cadmium ion absorption, Int. J. Biol. Macromol. 117 (2018) 1–6, https://doi.org/10.1016/j.ijbiomac.2018.05.159.
[98] Theng, B.K.G. Formation and properties of clay-polymer complexes, 2nd ed.; Elsevier: Amsterdam, The Netherlands, 2012.

[99] M. Fatnassi, C.-H. Solterbeck, M. Es-Souni, Clay nanomaterial thin film electrodes for electrochemical energy storage applications, RSC Adv. 4 (2014) 46976–46979, https://doi.org/10.1039/C4RA04330H.
[100] H. Zhao, C.H. Zhou, L.M. Wu, J.Y. Lou, N. Li, H.M. Yang, D.S. Tong, W.H. Yu, Catalytic dehydration of glycerol to acrolein over sulfuric acid-activated montmorillonite catalysts, Appl. Clay Sci. 74 (2013) 154–162, https://doi.org/10.1016/j.clay.2012.09.011.
[101] P.S. Nayak, B.K. Singh, Instrumental characterization of clay by XRF, XRD and FTIR, Bull. Mater. Sci. 30 (2007) 235–238, https://doi.org/10.1007/s12034-007-0042-5.
[102] H. Malektaj, A.D. Drozdov, E. Fini, J.d.C. Christiansen, The effect of pH on the viscoelastic response of Alginate–Montmorillonite nanocomposite hydrogels, Molecules 29 (244) (2024), https://doi.org/10.3390/molecules29010244.
[103] Z.Q. Xiong, X.D. Li, F. Fu, Y.N. Li, Performance evaluation of laponite as a mud-making material for drilling fluids, Pet. Sci. 16 (2019) 890–900, https://doi.org/10.1007/s12182-018-0298-y.
[104] Sapalidis, A.A.; Katsaros, F.K.; Kanellopoulos, N.K. PVA/Montmorillonite Nanocomposites: Development and Properties. Nanocomposites and Polymers with Analytical Methods. London: IntechOpen. 2011, 29–50. https://doi.org/10.5772/18217.
[105] Z. Jing, X. Dai, X. Xian, X. Du, M. Liao, P. Hong, Y. Li, Tough, stretchable and compressive alginate-based hydrogels achieved by non-covalent interactions, RSC Adv. 10 (2020) 23592–23606, https://doi.org/10.1039/D0RA03733H.
[106] G. Kowalski, M. Witczak, Ł. Kuterasiński, Structure effects on swelling properties of hydrogels based on sodium alginate and acrylic polymers, Molecules 29 (2024) 1937, https://doi.org/10.3390/molecules29091937.
[107] Z. Wang, Y. Huang, M. Wang, G. Wu, T. Geng, Y. Zhao, A. Wu, Macroporous calcium alginate aerogel as sorbent for Pb^{2+} removal from water media, J. Environ. Chem. Eng. 4 (3) (2016) 3185–3192, https://doi.org/10.1016/j.jece.2016.06.032.
[108] T. Nakajima, K. Hoshino, H. Guo, T. Kurokawa, J.P. Gong, Experimental verification of the balance between elastic pressure and ionic osmotic pressure of highly swollen charged gels, Gels 7 (2) (2021) 39, https://doi.org/10.3390/gels7020039.
[109] J. Siepmann, N.A. Peppas, Modeling of drug release from delivery systems based on hydroxypropyl methylcellulose (HPMC), Adv. Drug Deliv. Rev. 48 (2–3) (2001) 139–157, https://doi.org/10.1016/S0169-409X(01)00112-0.
[110] R.W. Korsmeyer, R. Gurny, E. Doelker, P. Buri, N.A. Peppas, Mechanisms of solute release from porous hydrophilic polymers, Int. J. Pharm. 15 (1) (1983) 25–35, https://doi.org/10.1016/0378-5173(83)90064-9.
[111] I.F. Shakoor, G.K. Pamunuwa, D.N. Karunaratne, pH-dependent release properties of curcumin encapsulated alginate nanoparticles in skin and artificial sweat, J. Natl. Sci. Found. 51 (3) (2023) 319–328, https://doi.org/10.4038/jnsfsr.v51i3.11221.
[112] P.L. Ritger, N.A. Peppas, Transport of penetrants in the macromolecular structure of coals. 4. Models for analysis of dynamic penetrant transport, Fuel 66 (6) (1987) 816–822, https://doi.org/10.1016/0016-2361(87)90130-X.
[113] C. Ulker Turan, Y. Guvenilir, Electrospun poly(ω-pentadecalactone-co-ε-caprolactone)/gelatin/chitosan ternary nanofibers with antibacterial activity for treatment of skin infections, Eur. J. Pharm. Sci. 170 (2022) 106113, https://doi.org/10.1016/j.ejps.2021.106113.
[115] P. Gurikov, I. Smirnova, Non-conventional methods for gelation of alginate, Gels 4 (2018) 14, https://doi.org/10.3390/gels4010014.
[116] Z. Guo, D. Zhao, Y. Li, et al., Solution chemistry effects on sorption behavior of cd (II) on ca-montmorillonite, J. Radioanal. Nucl. Chem. 288 (2011) 829–837, https://doi.org/10.1007/s10967-011-0998-x.
[117] S.S. Gupta, K.G. Bhattacharyya, Immobilization of Pb(II), cd(II) and Ni(II) ions on kaolinite and montmorillonite surfaces from aqueous medium, J. Environ. Manag. 87 (1) (2008) 46–58, https://doi.org/10.1016/j.jenvman.2007.01.048.
[118] M. Kuczajowska-Zadrożna, U. Filipkowska, T. Jóźwiak, Adsorption of cu(II) and cd(II) from aqueous solutions by chitosan immobilized in alginate beads, J. Environ. Chem. Eng. 8 (4) (2020) 103878, https://doi.org/10.1016/j.jece.2020.103878.
[119] K. Adamiak, A. Sionkowska, State of innovation in alginate-based materials, Mar. Drugs 21 (6) (2023) 353, https://doi.org/10.3390/md21060353.
[120] Y. Zhao, L. Zhan, Z. Xue, K.K.K. Yusef, H. Hu, M. Wu, Adsorption of Cu^{2+} and Cd^{2+} from wastewater by sodium alginate modified materials, J. Chemother. (2020) 5496712, https://doi.org/10.1155/2020/5496712.
[121] Barbier F. Duc G. Petit-Ramel M. Adsorption of lead and cadmium ions from aqueous solution to the montmorillonite/water interface Colloids Surf. A Physicochem. Eng. Asp. 2000 166 1–3 153 159 https://doi.org/10.1016/S0927-7757(99)00501-4.
[122] B. Ren, C. Shu, Z. Chen, Q. Xiao, Y. He, Adsorption and immobilization of cadmium by an Iron-coated montmorillonite composite, Water 16 (2024) 3105, https://doi.org/10.3390/w16213105.
[123] S.R. Kuchekar, M.P. Patil, H.R. Aher, V.B. Gaikwad, S.H. Han, Adsorptive removal of cadmium (II) ion from industrial wastewater by natural adsorbent, J. Mater. Environ. Sci. 10 (11) (2019) 1117–1122.
[124] J.S. Essomba, J. Ndi Nsami, P.D. Belibi Belibi, G.M. Tagne, J. Ketcha Mbadcam, Adsorption of cadmium(II) ions from aqueous solution onto kaolinite and metakaolinite, Pure Appl. Chem. Sci 2 (2014) 11–30, https://doi.org/10.12988/pacs.2014.31017.
[125] Z. Li, T. Katsumi, S. Imaizumi, X. Tang, T. Inui, Cd(II) adsorption on various adsorbents obtained from charred biomaterials, J. Hazard. Mater. 183 (2010) 410–420, https://doi.org/10.1016/j.jhazmat.2010.07.040.
[126] Y. Asci, M. Nurbas, Y.S. Acikel, Sorption of cd(II) onto kaolin as a soil component and desorption of cd(II) from kaolin using rhamnolipid biosurfactant, J. Hazard. Mater. 139 (2007) 50–56, https://doi.org/10.1016/j.jhazmat.2006.06.004.
[127] R. Foroutan, A. Tutunchi, M. Foroughi, B. Ramavandi, Efficient fluoride removal from water and industrial wastewater using magnetic chitosan/β-cyclodextrin aerogel enhanced with biochar and MOF composites, Sep. Purif. Technol. 363 (2) (2025) 132128.
[128] R. Foroutan, A. Tutunchi, A. Foroughi, B. Ramavandi, Defluorination of water solutions and glass industry wastewater using a magnetic pineapple hydrochar nanocomposite modified with a covalent organic framework, J. Environ. Manag. 377 (2025) 124651, https://doi.org/10.1016/j.envman.2025.124651.
[129] R. Foroutan, R. Mohammadi, J. Razeghi, M. Ahmadi, B. Ramavandi, Amendment of Sargassum oligostum biochar with MnFe2O4 and lanthanum MOF obtained from PET waste for fluoride removal: a comparative study, Environ. Res. 251 (1) (2024) 118641, https://doi.org/10.1016/j.envres.2024.118641.
[130] A. Massrour, S.J. Peighambardoust, M. Foroughi, R. Foroutan, B. Ramavandi, Crystal violet removal by sodium alginate-g-polyacrylamide/hydroxyapatite/cu-Fe LDH nanocomposite, Environ. Technol. Innov. 38 (2025) 104149, https://doi.org/10.1016/j.eti.2025.104149.
[131] R. Leyva-Ramos, L.A. Bernal-Jacome, I. Acosta-Rodriguez, Adsorption of cadmium(II) from aqueous solution on natural and oxidized corncob, Sep. Purif. Technol. 45 (2005) 41–49, https://doi.org/10.1016/j.seppur.2005.02.005.
[133] S. Cataldo, N. Muratore, S. Orecchio, A. Pettignano, Enhancement of adsorption ability of calcium alginate gel beads towards Pd(II) ion. A kinetic and equilibrium study on hybrid Laponite and montmorillonite–alginate gel beads, Appl. Clay Sci. 118 (2015) 162–170, https://doi.org/10.1016/j.clay.2015.09.014.
[134] M. Etcheverry, V. Cappa, J. Trelles, G. Zanini, Montmorillonite-alginate beads: natural mineral and biopolymers based sorbent of paraquat herbicides, J. Environ. Chem. Eng. 5 (6) (2017) 5868–5875, https://doi.org/10.1016/j.jece.2017.11.018.
[135] H. Kaşgöz, A. Durmuş, A. Kaşgöz, Enhanced swelling and adsorption properties of AAm-AMPSNa/clay hydrogel nanocomposites for heavy metal ion removal, Polym. Adv. Technol. 19 (2008) 213–220, https://doi.org/10.1002/pat.999.
[136] C.E. Brunchi, S. Morariu, Laponite®—from dispersion to gel—structure, properties, and applications, Molecules 29 (2823) (2024), https://doi.org/10.3390/molecules29022823.
[137] A. Rapacz-Kmita, M. Gajek, M. Dudek, R. Kurpanik, S. Kluska, E. Stodolak-Zych, Neomycin intercalation in montmorillonite: the role of ion exchange capacity and process conditions, Materials 17 (2024) 4207, https://doi.org/10.3390/ma17174207.
[138] Z.Q. Xiong, X.D. Li, F. Fu, et al., Performance evaluation of laponite as a mud-making material for drilling fluids, Pet. Sci. 16 (2019) 890–900, https://doi.org/10.1007/s12182-018-0298-y.